



UNIVERSITA' DEGLI STUDI DI NAPOLI "FEDERICO II"  
FACOLTA' DI SCIENZE MATEMATICHE, FISICHE E NATURALI  
DOTTORATO DI RICERCA IN SCIENZE DELLA TERRA  
XXI CICLO  
INDIRIZZO GEOFISICA

*HIGH-FREQUENCY GROUND MOTION  
AND ATTENUATION RELATIONSHIPS  
IN SOUTHERN ITALY*

Relatore  
*Ch.mo Prof.* Antonio Rapolla  
Relatore Esterno  
*Dr.* Aybige Akinci

Dottorando  
Sebastiano D'Amico

ANNO ACCADEMICO 2007-2008



## TABLE OF CONTENTS

<i>Chapter I</i>	
<i>Introduction</i> .....	3
<i>Chapter II</i>	
<i>Tectonic setting and data set</i> .....	10
<i>Chapter III</i>	
<i>Evaluation of the Regional Scaling Relationships</i> .....	36
<i>Chapter IV</i>	
<i>An Attenuation Relationship for Southern Italy</i> .....	50
<i>Chapter V</i>	
<i>Conclusion</i> .....	63
<i>References</i> .....	66



## ***CHAPTER I***

### ***Introduction***

The assessment of seismic hazard is probably the most important contribution of seismology to society. The prediction of the earthquake ground motion has always been of primary interest for seismologists and structural engineers. A deterministic approach is done by matching shape and amplitude of every single pulse in the seismograms. This point of view is very important in seismology, since it allows us to obtain important information about the seismic source, and also a quantitative description of the medium through which the energy propagates. Large earthquakes that have occurred in recent years in densely populated areas of the world (Izmit, Turkey, 17 August 1999; Duzce, Turkey, 12 November 1999; Chi-Chi, Taiwan 20 September 1999, Bhuj, India, 26 January 2001; Sumatra 26 December 2004) dramatically highlighted the inadequacy of a massive portion of the buildings erected in and around the epicentral areas. The Izmit event was particularly destructive because a large number of buildings were unable to withstand even moderate levels of ground shaking, demonstrating poor construction criteria and, more generally, the inadequacy of the application of building codes for the region. Building earthquake-resistant structures and retrofitting old buildings on a national scale may be extremely costly and may represent an economic challenge even for developed western countries. Planning and design should be based on available national hazard maps, which, in turn, must be produced after a careful calibration of ground motion predictive relationships (Kramer, 1996) for the region. Updating existing hazard maps represents



one of the highest priorities for seismologists, both in terms of recomputing the ground motion and of reducing the related uncertainties.

The quantitative estimate of the ground motion is obtained through the use of the so-called predictive relationships (see Kramer, 1996), which allow the computation of specific ground-motion parameter as a function of magnitude, distance from the source, and frequency and they should be calibrated in the region of interest. Those attenuation relationships are usually obtained regressing a large number of strong-motion data (Campbell and Bozorgnia, 1994; Boore *et al.*, 1993; Ambraseys, 1995, Ambraseys *et al.*, 1996, Ambraseys and Simpson, 1996; Sabetta and Pugliese, 1987, 1996). For the Italian region the most used attenuation relationships are those obtained by Sabetta and Pugliese (1987, 1996). They were the first author to present the result of a regression of strong motion data to define the attenuation of the peak horizontal acceleration (PHA) and peak horizontal velocities (PHV). The database used by Sabetta and Pgliese (1987) contained waveforms generated by events in different tectonic and geological environments. To obtain their equations Sabetta and Pugliese (1987) regressed the largest of the two peaks on the horizontal time histories; they generally uses the local magnitude. Sabetta and Pugliese(1996) developed empirical predictive relationships for the vertical and the horizontal components of the response spectra. The database used by both in the two papers (1987, 1996) had common components: Sabetta and Pugliese (1987) used 190 horizontal components from 17 earthquakes recorded in Italy since 1976 ( $4.6 < M < 6.8$ ); Sabetta and Pugliese (1996) used 95 accelerograms among the same data set. A multiple regression was carried out into the 1996 article for 14 different frequencies in the range 0.25–25 Hz.



Calabria, the toe of Italy on the Italian Peninsula, is part of the most active seismic belt in Italy and has a high earthquake hazard. Historical severe earthquakes are reported in the region (Boschi et al. 1995). The high seismic potential of the area, its population density and the inadequacy of some of the buildings make South Italy an area of high seismic risk where modern hazard studies are needed. The attenuation properties of the crust can be evaluated using the background seismicity as suggested by Chouet et al. (1978) and later demonstrated by Raoff et al. (1999) and Malagnini et al. (2000). In other words, it becomes possible to develop regionally-calibrated attenuation relationships even where strong-motion data are not available. The purpose of this work is to describe quantitatively the regional attenuation and source characteristics for constraining the amplitude of strong motion expected from future earthquakes in the area. In this work we use the background seismicity to perform our analysis (details in Malagnini et al. 2000). For each seismogram the logarithm of its peak value is written as the sum of an excitation term relative to an arbitrary reference distance, a site term, and a propagation term:

$$\log A(f, r) = EXC(f, r) + SITE(f) + D(r, r_{ref}, f)$$

As discussed later we compute the crustal attenuation parameter and factors related to the excitation term. A modeling is also carried out through the use of Random Vibration theory (RVT) (Cartwright and Louguent-Higgins, 1956) to obtain a functional form describing the empirical excitation and the distance-scaling relationships. Using the source and attenuation parameters estimated in this study and a set of programs called stochastic Model SIMulation (SMSIM: Boore, 1996) it is possible to predict the



expected ground shaking in term, for example, of PGA. We also derive a functional form for a predictive relationship in the study area.

This kind of studies are usually calibrated on “rock-site”. It is really important highlight that, from an engineering point of view, it is necessary also consider the characteristic of a specific site, the so called site effects (Rapolla et al. 2008). In fact, they are very important and can affect a lot the constructions. In this contest the liquefaction (Kramer, 1996) play a key role. Liquefaction may occur when soil deposits have lost their strength and behave as a viscous liquid rather than as a solid. It reduces the strength of the soil to the point where it causes the building to collapse or to be unstable, empty buried tanks to rise to the surface, slope failures, lateral spreading, surface subsidence, ground cracking and sand blows. Earthquake liquefaction has caused significant damage and is also one major earthquake hazard in different part of the world. The effect of amplification/deamplification at a site, due to the surface geology and subsurface structure, should be considered in ground motion evaluation at the site. To estimate the site amplification/deamplification different method are proposed (King and Tucker, 1984; Field and Jacob, 1995; Malagnini et al. 2004, 2007; Stiedl et al., 1996; Moya et al., 2000). Amplification and deamplification due to surface geology of a particular site is a quite complex phenomenon which also depends on the frequency and the level of the ground motion. However a lot of studied are carried out to investigate the site response (Carrara and Rapolla, 1987; Rapolla 2004; Rapolla et. 2002; 2008).

The obtained results can be used for engineering design. We use the same methodology for data processing and analysis as before did in different part of the world: California (Raoff et al. 1999; Malagnini et al. 2007), northwestern United



States (Herrmann and Dutt, 1999; Jeon and Herrmann 2004), central United States (Herrmann and Malagnini, 1996), Mexico (Ortega *et al.*, 2003), Greece and Crete (Pino *et al.*, 2001), Italy (Malagnini *et al.*, 2000a,c: 2002; Morasca *et al.* 2006; Scognamiglio *et al.* 2005), Central Europe (Malagnini *et al.*, 2000b, Bay *et al.*, 2003), Turkey (Akinici *et al.*, 2001, 2006), India (Bodin *et al.*, 2004). The approach has been largely applied in Italy but, due to the “poor” distribution of seismic station in Southern Italy, the area was not yet resolved from this point of view. Fortunately, the deployment of a large number of seismic stations in the area allows us to have a good data set for performing the necessary analysis and find a suitable attenuation relationship for Southern Italy. Preliminary results were firstly presented at the Seismological Society of America meeting (Akinici *et al.* 2007). The results are obtained in this study are useful to implement tools like *Shake Map* (Wald *et al.* 2005) which need also this kind of information to generate an earthquake response.

ShakeMap is a tool used to portray the extent of potentially damaging shaking following an earthquake. It can be found on the Internet and is automatically generated for both small and large earthquakes in areas where it is available. It can be used for emergency response, loss estimation, and public information. ShakeMap was first developed for earthquakes in southern California. Istituto Nazionale di Geofisica e Vulcanologia (INGV) runs this tools for Mediterranean earthquake and in particular for the Italian ones. Shake Map shows the distribution of ground shaking in the region, information critical for emergency management decision making. It is the distribution of intensity rather than the magnitude that provides useful information about areas prone to damage. Having this information in real time will result in lives saved and reduction in property damage. After a damaging earthquake, emergency



managers must quickly find answer to important questions such as the localization of the most serious damage, and the area with the less one; the resources that must be mobilized and in what quantity, Usually Government response organizations answer these questions after a preliminary survey of the damaged area. This reconnaissance can require several hours or sometimes some days to be completed. As a result, decisions regarding search and rescue, medical emergency response, care and shelter for the injured and displaced persons, and other critical response needs must often be made while information is still incomplete. In this context a rapid and automatic response for the injured area is really important, that is why attenuation relationship are really important in similar tools.

Ground motion attenuation relationships may be determined in two different ways: empirically, using previously recorded ground motions, or theoretically using seismological models to generate synthetic ground motions that account for source, site and path effects,

In the present thesis the first chapter present a brief introduction on the problem issued in this work and the motivation. The second chapter provides a description of the tectonic of the area and the data and seismic instruments used to develop; it also presents some examples of moment magnitude inversion for a couple of the largest events in the used data-set. The third chapter briefly present the methodology firstly described by Raouf et al. (1999) and here used; there are also reported the results obtained applying the methodology and the predicted ground motion scaling results computed using the SMSIM programs (Boore, 1996). Chapter four reports the approach developed to derive a predictive ground motion relationship for southern



Italy obtained by performing the regression of the Peak Ground Acceleration (PGA) data. The fifth chapter summarizes to the conclusion of the present work.



## **CHAPTER II**

### ***Tectonic setting and data set***

#### ***2.1 Tectonics***

The Italian peninsula across the Mediterranean Sea is part of the tectonic plate boundary between the Eurasian and the African plates, which continue to move closer to each other. The Calabrian Subduction System results from the fragmentation of formerly continuous Western Mediterranean subduction zone. It developed in a geodynamic setting characterized by N-S convergence between Africa and Eurasia, and by a strong rollback of the slab that induced the opening of back arc extensional basins (Gueguen et al., 1998; Faccenna et al., 2001). This motion controls the long-term evolution of the boundary, but recent geologic changes suggest a more rapid tectonic event superimposed on the slow motion of the big plates and localized to the Apennine arc. This signature event of the Italian peninsula is most dramatically manifested in the current deformation along the Calabrian portion of the arc. From a geodynamic point of view southern Italy is divided into two regions. The Southern one, the so-called Calabrian Arc, is the area where the Ionian lithosphere subducts beneath the Tyrrhenian Sea; the subduction is characterized by an eastward rollback (e.g., Malinverno and Ryan, 1986; Doglioni *et al.*, 1996). North of the Calabrian Arc there are the so-called Southern Apennines that constitute the accretionary prism of the Adriatic plate subduction (e.g., Doglioni *et al.*, 1996, and references therein); on the basis of geological evidence the hinge of this subduction has been migrating northeastward up to the Pliocene; at present it is thought to be quiescent. The tectonic of the Southern Apennines is dominated by a NE-SW oriented tensile stress field



(Amato and Montone, 1997). The latter generates a series of normal fault systems with longitudinal trend. The Calabrian Arc in its northern portion has an almost North-South trend. It is also apparently characterized by extensional activity oriented along its axis. Strong lateral heterogeneity affects the southern Tyrrhenian lithosphere (Morelli et al., 1975; Calcagnile et al., 1979, 1982; Calcagnile and Panza, 1981; Scarpa, 1982; Steinmetz et al., 1983; Panza et al., 1990; Amato et al., 1993). One of the main features is the thickening of both the crust and lid from the abyssal plain to the Calabrian Arc (Figs. 2.1 and 2.2), which is also related to a decrease in surface heat flow (El All and Giese, 1978; Loddo and Mongelli, 1979; Mongelli et al., 1989) and gravity (Colombi et al., 1973; Mongelli et al., 1975). With regard to thermal conditions, El All and Giese (1978) have also reported the isotherm patterns in vertical sections (Fig. 2.2). Geological studies (Frazzetta et al., 1982; Ghisetti and Vezzani, 1982) and DSS surveys (Finetti and Del Ben, 1986) revealed the dominant presence of almost NW-SE transcurrent faults in the southern Tyrrhenian area, showing dextral mechanism in the southernmost sector (Filicudi, Sisifo, Vulcano and Taormina faults, Fig. 2.1) and left mechanism to the north (Palinuro and Policastro faults, same figure). The situation is rather more complex in the confining sectors, such as in the Calabrian Arc where different types of mechanisms are present. Nevertheless, graben-like structures parallel to the Arc (Fig. 2.1) are of special concern because they have been the site of the most intense (magnitudes 6 to 7) regional earthquakes in the last centuries (Ghisetti and Vezzani, 1982; Martini and Scarpa, 1982; Mulargia and Boschi, 1982; Ghisetti, 1992). The lithosphere beneath the southern Tyrrhenian Sea is characterized by a lower level of seismic activity, with maximum magnitudes in the range 5-6 (Falsaperla et al., 1989).

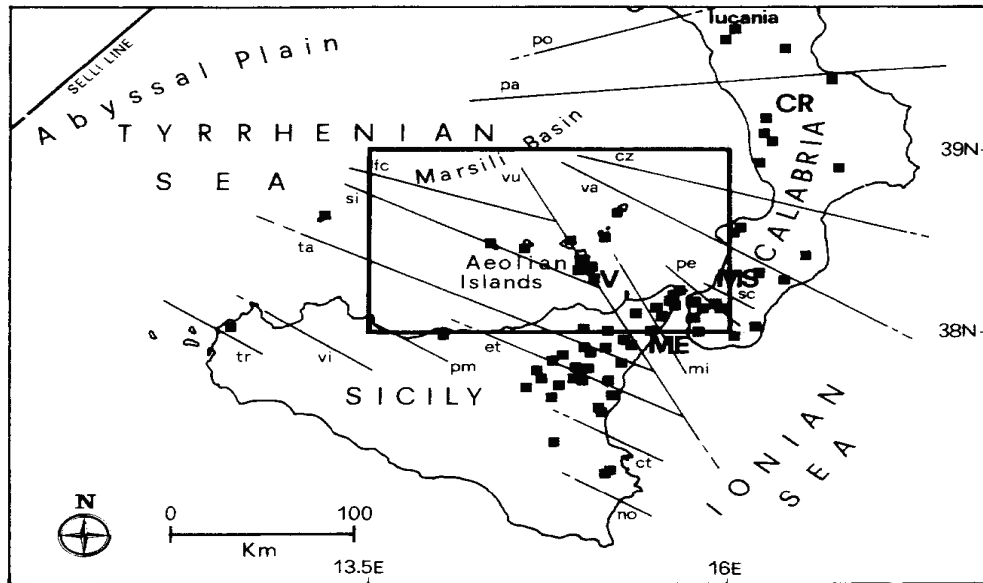


Fig. 2.1: Location of the seismic stations used in the Neri et al. (1996) paper; there are also present the main fault systems in the region (tr=Trapani, no=Noto; ri=S. Vito; pm=Palermo; ct= Catania; et = Etna; ta – Taormina; si=Sisifo; fc=Filicudi; vu = Vulcano; cz = Catanzaro; pa = Palinuro; po=Policastro; ME, MS and CR=Messina, Mesima and Crati grabens: data from Ghisetti and Vezzani, 1982 and Finetti and De/ Ben, 1986). V indicates the location of Vulcano Island. The rectangle represents the area where seismological investigation were conducted by Neri et al. 1996.

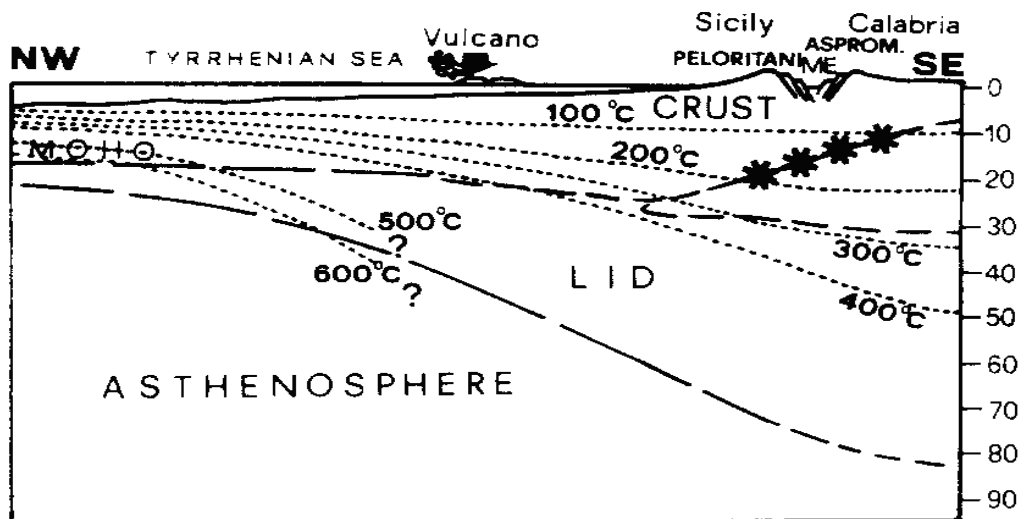


Fig. 2.2: NW-SE vertical section passing through Vulcano Island with the indication of isotherms (El All and Giese, 1978), the Moho depth and the lithosphere thickness (basic data are from Calcagnile and Panza, 1981). Asterisks indicate the location beneath the Calabrian Arc of the thrust front of the southern Tyrrhenian crust on the Ionian one according to Ghisetti (1984): thrusting is considered to occur in a ductile (and thus aseismic) environment by the same author. ME indicates the location of the Messina graben.

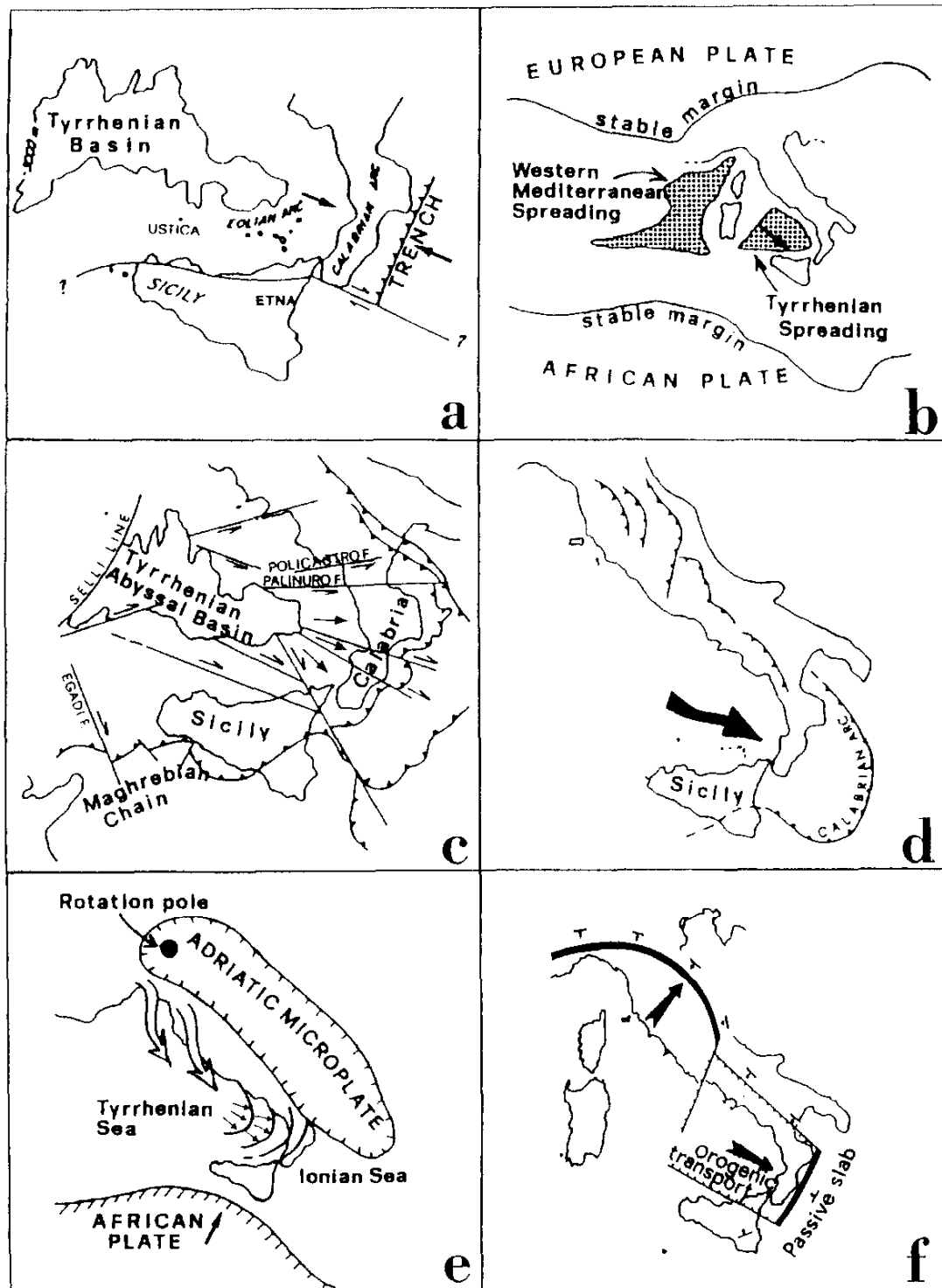


Fig. 2.3: Sketch map of several tectonic models proposed in the literature for the southern Tyrrhenian region (a: Barberi et al., 1973; b: Scandone and Patacca, 1984; c: Finetti and Del Ben, 1986; d: Locardi, 1988; e: Mantovani et al., 1990; f: Patacca et al., 1990). A common feature of all models and relevant for our study is the Southeastward kinematics of the southern Tyrrhenian lithosphere. This is indicated by full arrows in all model representations and has a different origin in the different models (obduction, rifting, mantle diapir growth, etc.). The picture comes from Neri et al. 1996.



An additional seismic feature of the southern Tyrrhenian region is deep earthquake activity along a Northwestward dipping Benioff plane (Peterschmitt, 1956: Caputo et al., 1970: Gasparini et al., 1982: Anderson and Jackson, 1987). Deep seismicity is one of the features which led Barberi et al. (1973) to hypothesize the existence of an active subduction process in the region and to interpret the southern Tyrrhenian area as a back-arc basin. More recently, other tectonic investigations and models have been proposed (Cristolblini et al., 1985: Finetti and Del Ben, 1986: Malinverno and Ryan, 1986: Rehault et al., 1987: Lavecchia, 1988: Locardi, 1988: Mascle et al., 1988: Savelli, 1988: Boccaletti et al., 1990; Mantovani et al., 1990: Patacca et al., 1990: Van Dijk and Okkes, 1991: Nur et al., 1993) and some of them are schematically represented in Fig. 2.3. Rifting processes have been hypothesized by Scandone and Patacca (1984), Finetti and Del Ben (1986). Patacca and Scandone (1989) and Patacca et al. (1990). Patacca et al. (1990) interpret deep earthquakes as related to passive subduction of a Ionian lithosphere slab which was active before the Tyrrhenian opening (Middle-Upper Miocene). In this model, eastward roll-back of the Ionian lithosphere would produce the relaxation of the Tyrrhenian lithosphere and thrusting of the latter onto the former. This mechanism is fundamental to the development of the opening process, as well as to (1) mountain building in the Calabrian Arc and (2) tensional stresses along the western margin of the Arc. Locardi (1988) proposes a model assuming the growth of mantle structures in the whole Tyrrhenian region. According to Mantovani et al. (1985, 1990), the dynamics of the Tyrrhenian region is controlled by the rotation of the Adriatic microplate around a pole located in the Alpine chain, in the framework of the northeastward compression exerted by the



African plate. In the frame of this ongoing debate, an important feature in all the above-mentioned models is the kinematics of the southern Tyrrhenian lithosphere, which would be affected by nearly southeastward movements, e.g. towards the Calabrian Arc (Fig. 2.3). According to Finetti and Del Ben (1986), these movements are related to an opening process along the Selli line (Figs. 2.1 and 2.3). The lithospheric mass migration may have been characterized by a gradually decreasing intensity since the Middle Pliocene and, in the most recent times, it seems to have mainly affected the most internal structures of the original front (Selli line). In the framework of the rifting dynamics, Patacca et al. (1990) maintain that an important episode of new crust generation probably started during the Lower Pleistocene in the Marsili basin (Fig. 2.1). A block drifting tectonics is suggested by Rehault et al. (1987) who propose a kinematic scheme similar to that of Finetti and Del Ben (1986). The Peloritani and Aspromonte chains located at the eastern boundary of the southern Tyrrhenian Sea (Calabrian Arc, Figs. 2.1 and 2.2) have been uplifting since Pleistocene at a rate of about 1 mm/yr (Burton, 1964; Ghisetti, 1980). According to Mulargia et al. (1984), this process has probably been taking place aseismically and seems to be confirmed, at present, by tidal and leveling measurements. However, marked subsidence episodes affect the Messina Strait graben (Figs. 2.1 and 2.2) during the most intense phases of local seismic activity (e.g. the sequence of 1908, maximum magnitude 7.0; Mulargia and Boschi, 1982; Mulargia et al., 1984; Bottari et al., 1989). Other major earthquakes of the Calabrian Arc (1783,  $M = 7.1$ ; 1905,  $M = 6.8$ ) have also been interpreted as related to the activity of the main graben structures of the Arc (Martini and Scarpa, 1982). The graben structures should approximately involve the upper crust while, below, thrusting of the Tyrrhenian crust onto the Ionian one is



thought to occur in a ductile, and therefore aseismic, environment (Ghisetti, 1984; Fig. 2.2).

## ***2.2 Data Set & Data Preparation***

The final data set analyzed in this paper consists of more than 10600 three/component seismograms from about 350 regional earthquakes, recorded from December 2003 and October 2005. The magnitude of the events ranged between  $M=2.5$  and  $M=4.7$ , whereas the path lengths ranged between a few kilometers and about 280 km. In this study we used seismic recording coming from two different projects: the SAPTEX (Southern APennines Tomography Experiment) (Cimini et al. 2006) and CAT-SCAN (Calabria Apennine Tyrrhenian – Subduction Collision Accretion Network) array; both are temporary experiments. Figure 2.4 shows the distribution of the seismic instruments location for the SAPTEX array in Southern Italy. The deployment of the portable digital seismographs started at the end of June 2001 and finished at the end of 2005, however the 2003 and the 2004 were the years with the maximum number of available seismic stations. The geometry of the array was spanned in Calabria, Aeolian islands and in the southern part of the Apulia (fig. 2.4). For each station we installed a 24 bit RefTek 72A07 digitizer, a three-components Lennartz 3D-5 s sensor (LE-3D/5s) with natural frequency and damping of 0.2 Hz and 0.70, respectively, a hard disk with capacity of 1, 2 or 4 Gb, two 70 Ah-12 V batteries, and two 45-Watt solar panels in sites where electrical power was unavailable. A GPS antenna provided the absolute timing for the recording. Digitizers were set to operate in continuous mode recording,



with unitary preamplifier gain and sampling rate of 50 sample per second (sps) to record both teleseisms and local/regional seismicity. For the output, we adopted record lengths of 3600 s (hourly files) and compressed data format, which required changing the 1-Gb hard disks about once a month at the noisiest stations (*e.g.*, volcanic sites). At 50 sps, the amount of uncompressed raw data produced by each station is about 52 Mb/day. The frequency response of the LE-3D/5 s extended band sensors (velocity response flat from 0.2 to 40 Hz, decaying with 40 db/decade below the natural frequency) and the chosen sampling rate of 50 sps allowed the recording of weak ground motions in the frequency band between about 0.1 and 20 Hz. In this band, the main sources of seismic noise are the sea (marine microseismic band 0.05-1 Hz), the wind, cultural noise, and the site tectonics.

The second set of data comes from the CAT-SCAN (Calabria Apennine Tyrrhenian – Subduction Collision Accretion Network) array (figure 2.5) deployed in southern Italy from 2004 and 2005. Researchers from the Lamont-Doherty Earth Observatory, Istituto Nazionale di Geofisica e Vulcanologia and University of Calabria, deployed almost 40 portable digital broadband seismographs throughout southern Italy. Each station was equipped with data logger Reftek130 or Reftek72A07 and different three-component sensors (cmg40t, cmg3t, l-22, sts2, trilium40, cmg3esp).

Figures 2.6. and 2.7 show the characteristic of the data set used during this study. They show the source-distance distribution (fig 2.6), the number of recording as a function of magnitude (fig. 2.7a) and as a function of depth (fig. 2.7b). In the present study we consider only the shallow events excluding from the original data set those ones had a depth greater than 40 km. Table 2.1 reports the sites description for both SAPTEX and

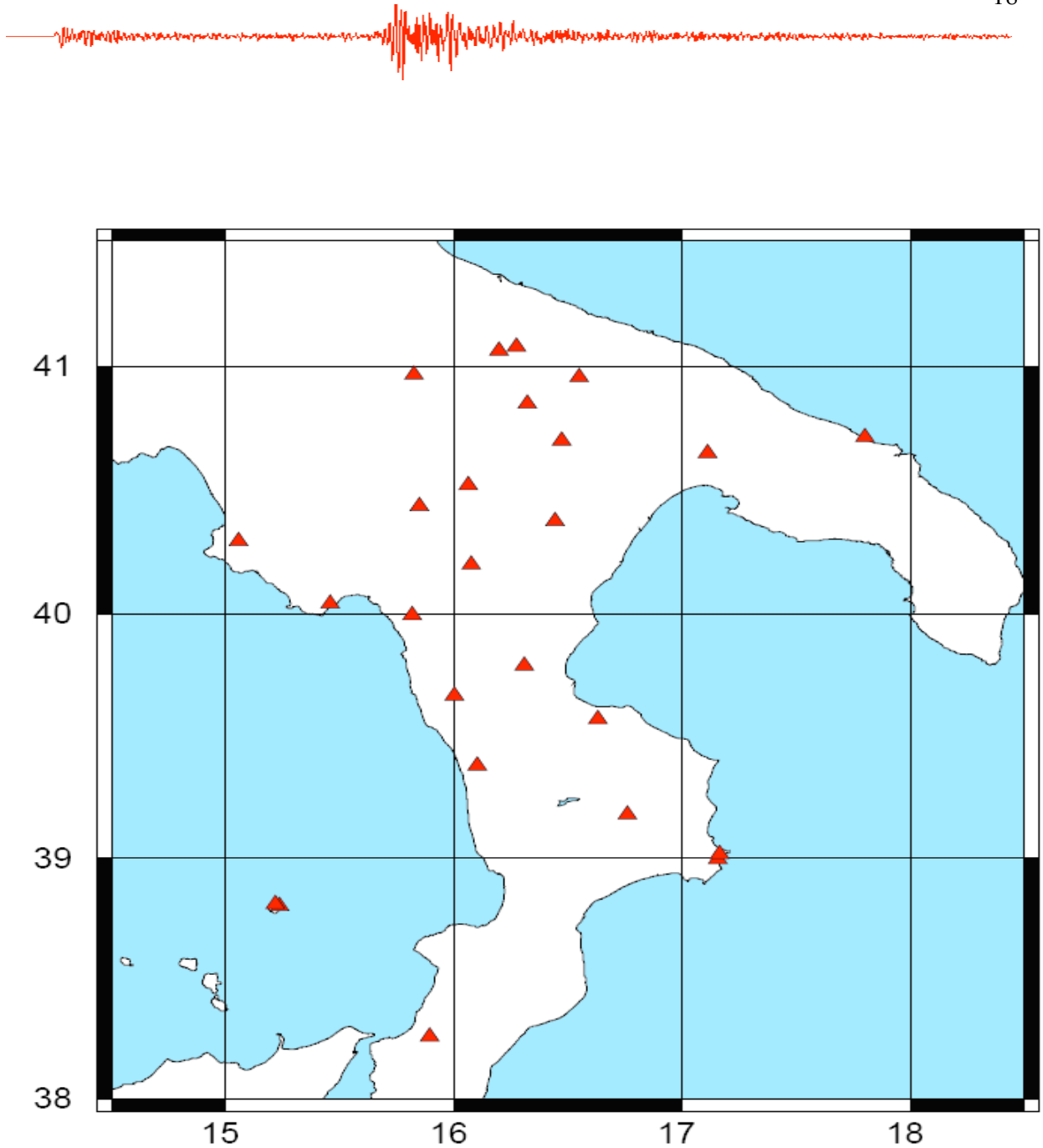


*Figure 2.4.: The figure reports the station distribution for the SAPTEX (Southern APennines Tomography Experiment) (Cimini et al. 2006). The SAPTEX array was planned with the main goal to better resolve the crustal and upper mantle structure beneath southern Italy. In this region the paucity is still remarkable.*

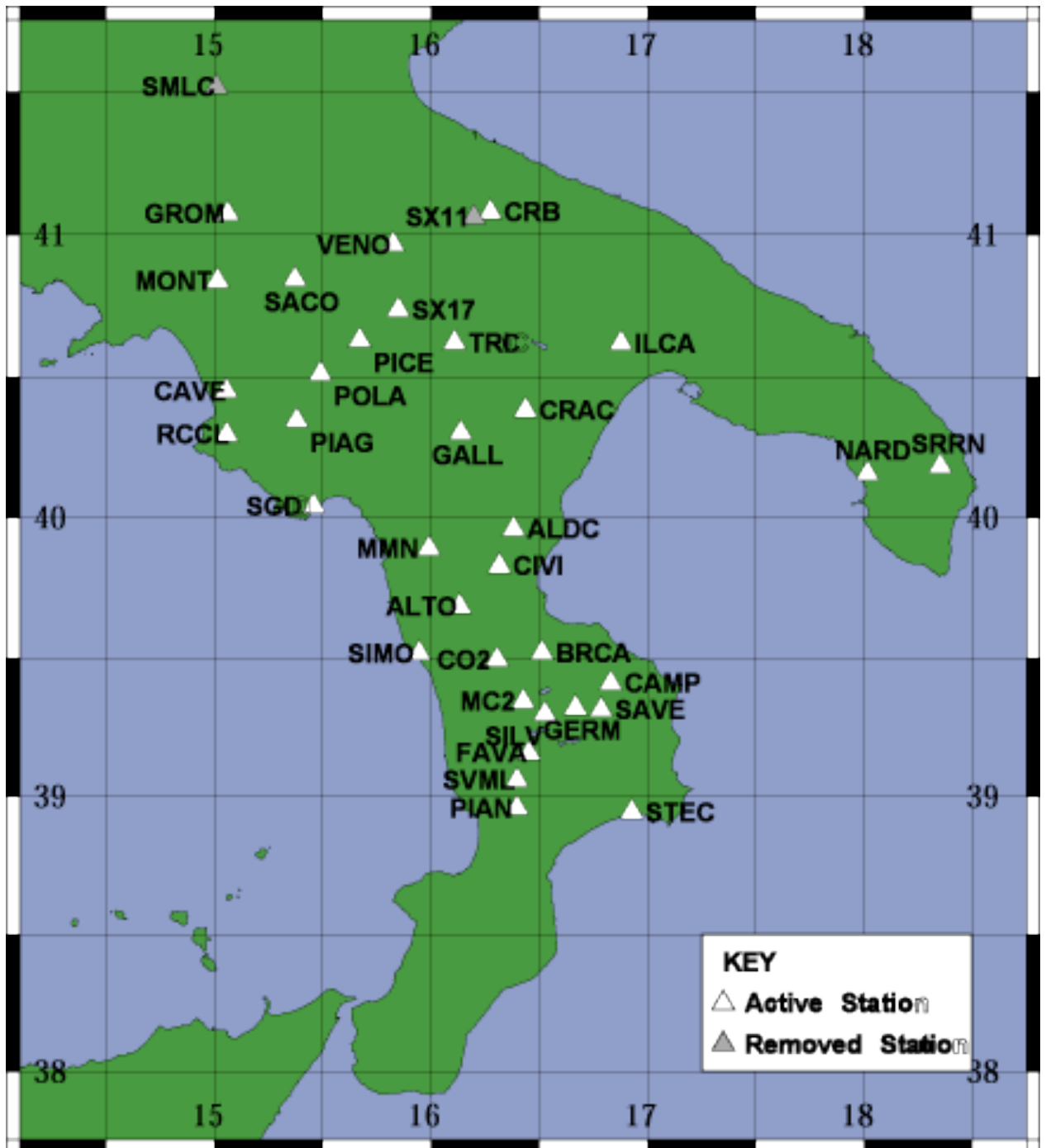


Figure 2.5: The map show the station distribution for the CAT-SCAN (Calabria Apennine Tyrrhenian – Subduction Collision Accretion Network) array deployed from 2004 and 2005 by a joint project among different Institutions: Istituto Nazionale di Geofisica e Vulcanologia, Lamont-Doherty Earth Observatory and the University of Calabria. The white triangles represent the active stations that recorded during the duration of the experiment, the grey triangles represent the removed stations. Data coming from the removed stations were not used in the present study. Note that two stations, SX11 and SX17 have the same name of two SAPTEX project stations.

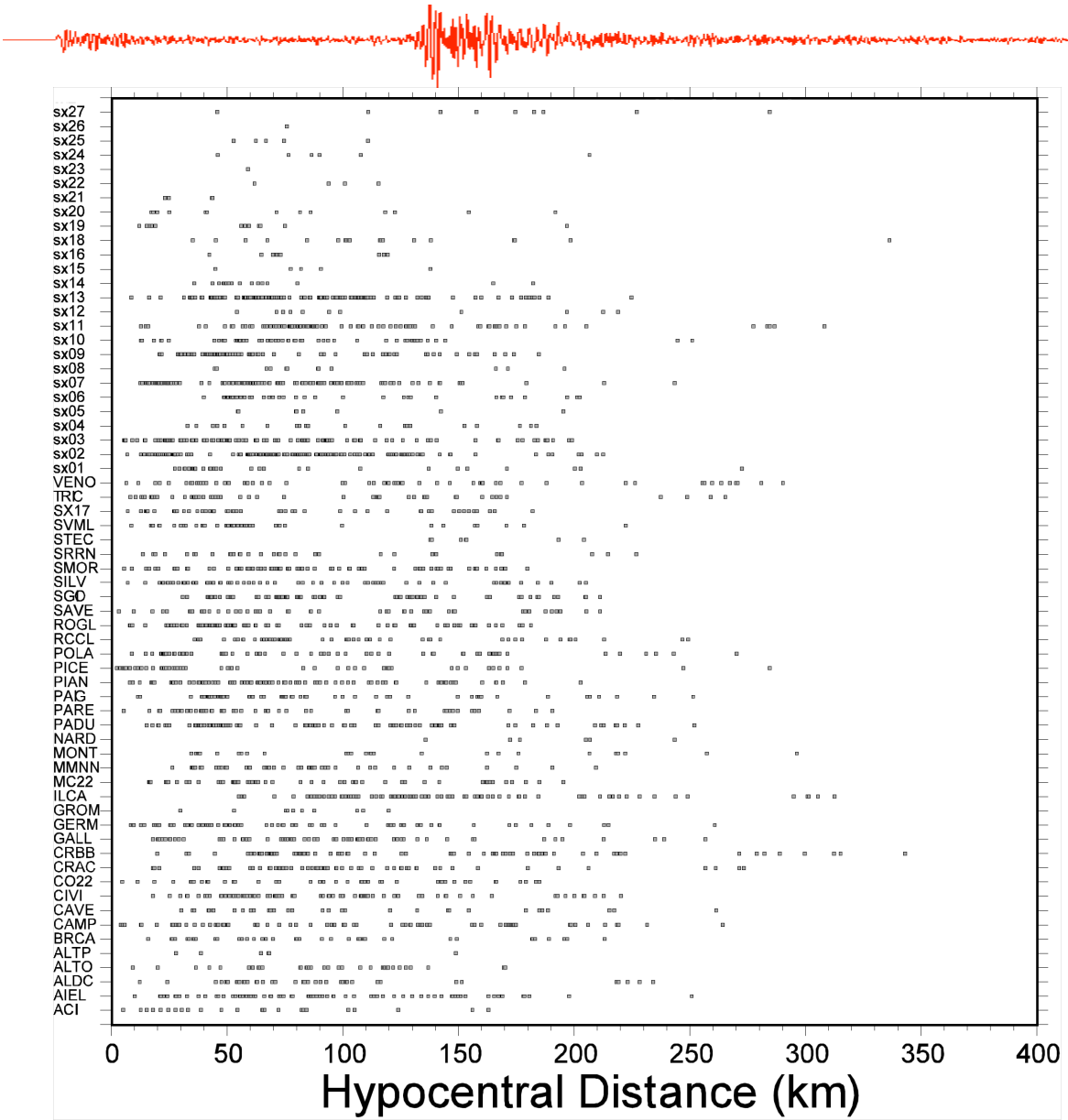


Figure 2.6: Source-receiver distance distribution

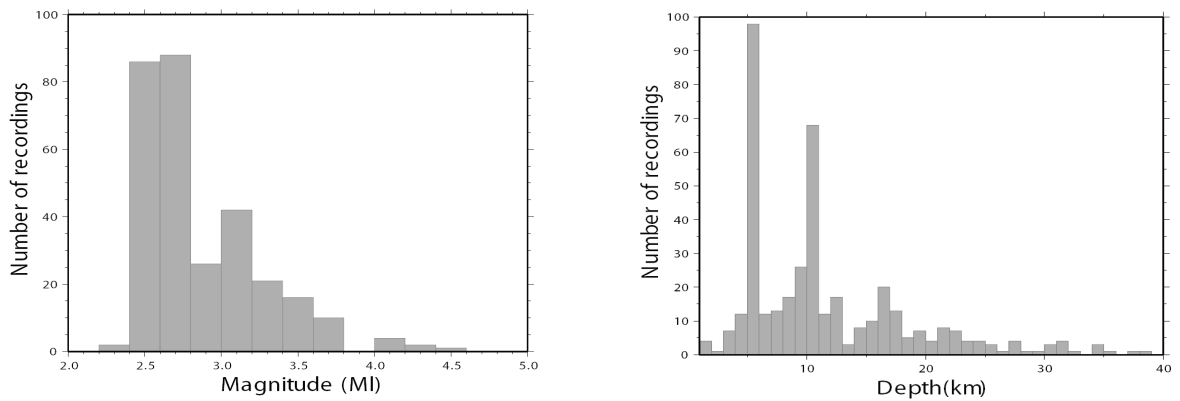


Figure 2.7: a) number of earthquake as a function of local magnitude; b) number of earthquake as a function of depth. In this study we did not consider the events with depth greater than 40km.

Table 2.1 Description of SAPTEX and CATSCAN sites.

Station	Site	Latitude (N)	Longitude(E)	Elev. (m)	Geology	Class. NEHR P
SX01	Castrocucco	39.99380	15.81556	665	Calcarenite	A
SX02	Timpagrande	39.17936	16.75829	810	Granite	A
SX03	S. Giovanni a Piro	40.04109	15.45744	585	Calcarenite	A
SX04	Castel del Monte	41.07758	16.27273	529	Limestone	A
SX05	Rocca Cilento	40.29556	15.05511	682	Conglomerate	A
SX06	S. Chirico Raparo	40.19924	16.07590	968	Sandstone and marl	B
SX07	Barisci	40.84924	16.32098	469	Conglomerate	A
SX08	Pietrapertosa	40.52148	16.06124	1077	Feldspatic sandstone	B
SX09	Craco	40.37643	16.44330	367	Clay	A
SX10	Picciano	40.69913	16.47064	481	Clay and marl	A
SX11	Minevino Murge	41.06109	16.19586	598	Limestone	A
SX12	S. Sosti	39.66635	16.00190	588	Dolomitic limestone	A
SX13	Venosa	40.96438	15.82344	460	Conglomerate	A
SX14	Montalto Uffugo	39.37976	16.10046	990	Schist	A
SX15	Stromboli	38.80264	15.23423	125	Basaltic lava	A
SX16	Quasano	40.95423	16.54832	520	Limestone	A
SX17	Pietragalla	40.73605	15.84764	870	Marl	A
SX18	Alicudi	38.53381	14.35637	156	Basaltic lava	A
SX19	Rossano	39.57064	16.63017	433	Phyllite	A
SX20	Celeste	38.26031	15.89393	694	Amphibolitic schist	A
SX21	Isola Capo Rizzuto	38.99696	17.15433	152	Sandstone	B
SX22	Cassano allo Jonio	39.78891	16.30720	473	Dolomitic limestone	A
SX23	Stromboli	38.80988	15.21803	165	Basaltic lava	A
SX24	Crotone	39.01600	17.16438	166	Sandstone	B
SX25	Massafra	40.64908	17.11090	431	Limestone	A
SX26	Carovigno	40.71468	17.79966	43	Limestone	A
XXXX XXXX						
ACII	Arcacavata di Rende	39.3590	16.2268	232	Marine deposits and calcarenite	B
AIEL	Aiello Calabro	39.1166	16.1581	314	Sandstones and calcarenite	B
ALDC	Alessandra del Carretto	39.9590	16.3813	998	Sandstones	B
ALTO	Altomonte	39.6828	16.1301	406	Marine deposits and calcarenite	B
ALTP	Altomonte	39.6979	16.1319	482	Marine deposits and calcarenite	B
BRCA	Baraccone	39.5164	16.5127	957	Granites and Granodiorites	A

CAMP	Campana	39.4076	16.8303	552	Marine deposits and calcarenite	B
CAVE		40.4490	15.0531	218		B
CIVI	Civita	39.8283	16.3150	399	Limestones	A
CO22		39.4926	16.3051	434	Marine deposits and calcarenite	B
CRAC	Craco	40.3815	16.4348	330	Clay	A
CRBB	Centro Ricerca Bonomo	41.0790	16.2721	495	Marine deposits and calcarenite	B
GALL	Gallicchio	40.3024	16.1365	804	Marine deposits and calcarenite	B
GERM	Germano	39.3203	16.6674	1226	Granites and Granodiorites	A
GROM		40.0727	15.0594	448	??????	?
ILCA	Castellaneta	40.6176	16.8772	308	Limestones	A
MC22	Moccone	39.3429	16.4250	1310	Granites and Granodiorites	A
MMNN	Mormanno	39.8909	15.9904	872	Limestones	A
MONT	Montella	40.8369	15.0140	782	Limestones and dolmites	A
NARD	Nardo	40.1547	18.0167	62	Carbonates	A
PADU	Padula	40.3334	15.6722	763	Limestones and dolomites	A
PARE	Parenti	39.1570	16.4522	1266	Granites and Granodiorites	A
PIAG	Piaggine	40.3461	15.3773	660	Shales and clays	A
PIAN	Pianopoli	38.9576	16.3968	378	Plio-Quaternary	B
PICE	Picerno	40.6291	15.6685	766	Limestones	A
POLA	Polla	40.5104	15.4879	512	Limestones	A
RCCL	Rocca Cilento	40.2956	15.0551	643	Sandstones	B
ROGL	Rogliano	39.1785	16.3260	652	Granites and anphybolites	A
SAVE	Savelli	39.3118	16.7841	954	Granites and Granodiorites	A
SGIO	San Giovanni a Piro	40.04109	15.45744	585	Calcarenite	A
SILV	Silvano	39.2978	16.5237	1487	Granites and Granodiorites	A
SIMO		39.5151	15.9444	154	Limestones and dolomites	A
SX17	Pietragalla	40.73605	15.84764	870	Marl	A
SMOR	San Morello	39.4930	16.8766	364	Sandstones and calcarenite	B
SRRN	Serrano	40.1822	18.3513	100	Limestones	A
STEC	Steccato di Cutro	38.9426	16.9257	17	Marine deposits and calcarenite	B
SVML	Soneria Mannelli	39.0590	16.3963	759	Granites	A
TRIC	Tricarico	40.6201	16.1070	722	Limestones	A

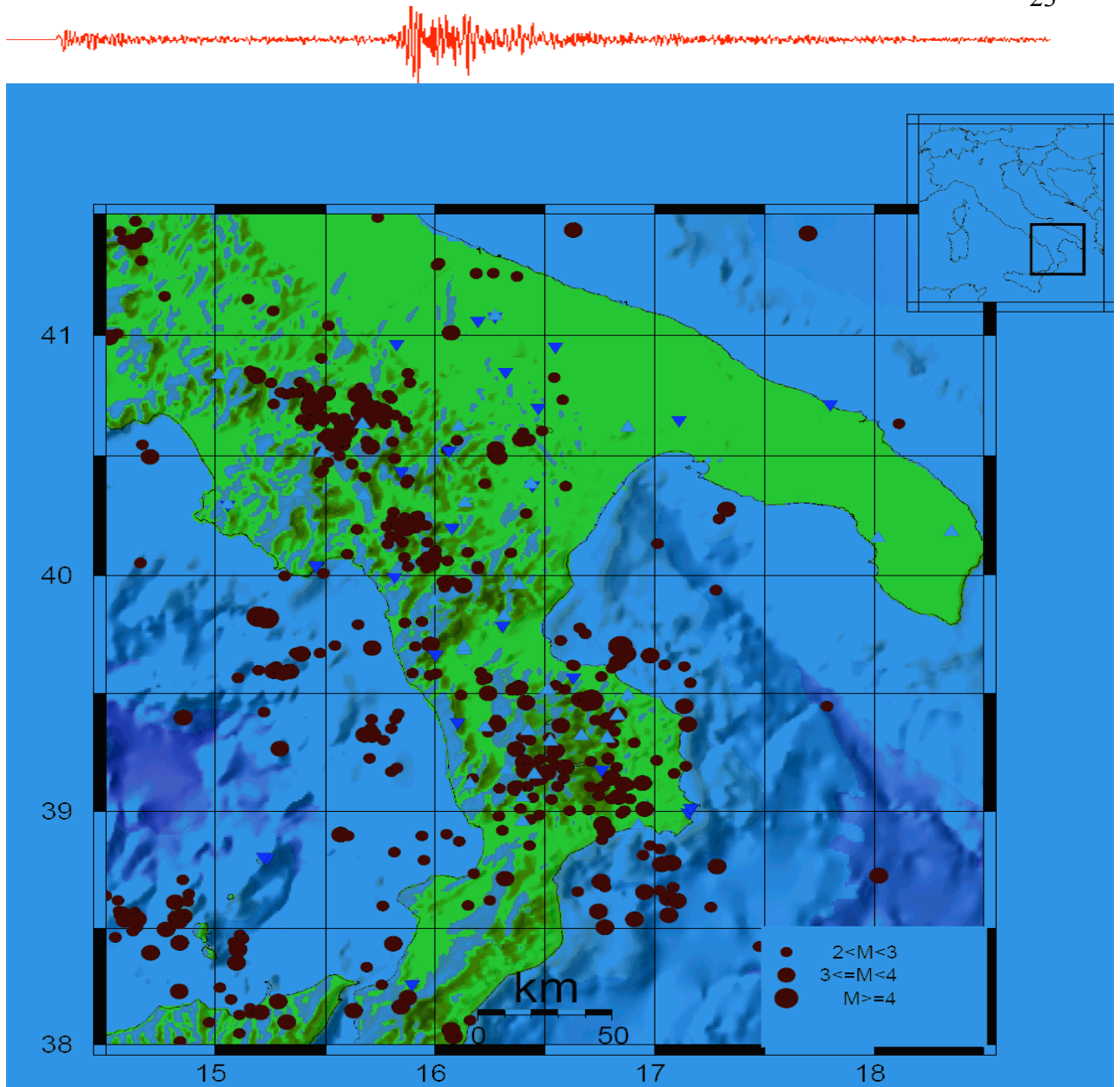


Figure 2.8 The map shows the epicentral distribution of the events (red dots) used in the present study. The size of the dots is proportional with the magnitude of the events. The with triangles are the station of the CATSCAN experiment while the blue ones are those belonging to the SAPTEX array.



CATSCAN. Each waveform is examined to eliminate those having low signal to noise ratio and/or anomalous glitches; every seismogram is corrected for instrument response to ground velocity in m/sec. The picking of P and S-arrivals are also reviewed. The digital data series were corrected for instrument response to form ground velocity in units of m/sec. This is done by a filtering operation within SAC (Seismic Analysis Code). The instrument response was given in the form of SAC pole-zero files. We also remove the linear trend in the data set, taper the beginning and end of the time series; the result is the velocity time series. Careful correction for instrument response is critical to this study since we will attempt to study the absolute scaling of ground motion generated by the source. The figure 2.8 reports all data an stations used in this study.

### ***2.3 Moment Tensor Solutions***

For quantitative studies of the earthquake source one may either compared observed to predicted seismograms by passing ground motion synthetics through a mathematical model of the seismic data acquisition system, or, comparing predicted ground motions to data derived estimates. Regional waveforms recorded by modern seismographs contain much information about the seismic source and the Earth between the source and each receiver. When low-pass filtered, the waveforms appear simple enough to be modelled using synthetic seismograms, such as generated using the programs distributed in *Computer Programs in Seismology* (Herrmann R.B. and Ammon C.J. 2002). This volume described a set of tools built upon the synthetic seismogram codes, to analyze source properties.



In this paragraph I will briefly report the moment tensor solutions for some events into the final data set. It is really important to know the moment magnitude (Mw) especially for the largest events into the data set. For this reason we computed the moment tensor solution for our largest events reported in table 2.2. In order to perform the analysis it is necessary compute the Green's functions. Two types of files must be created to implement the inversion techniques described in this tutorial. For a given regional Earth model, one consists of depth dependent files used for the surface-wave fundamental mode spectral amplitude studies and the other consists of SAC formatted time-series of basic Green's functions for a given source depth and epicentral distance. A general inversion of a three-component seismogram for source moment-tensor elements, requires just ten Green's functions. These can be generated by any of the synthetic seismogram techniques described in the overview. Each Green's function, stored as a SAC binary file (in the binary format of the local computer architecture), is a function of source depth and epicentral distance. This requires an organization that incorporated source depth and epicentral distance. The naming of the files is of the form *xxxxxddd.grn* where *xxxxx* denotes the epicentral distance, *ddd* denotes the source depth, and *grn* denotes one of the ten Green's functions.

Table 2.2

<b>Evt.Num.</b>	<b>Date</b>	<b>Origin Time</b>	<b>Longitude</b>	<b>Latitutde</b>	<b>Depth</b>	<b>MI</b>	<b>Mw</b>
1	2004/02/24	05:21:26	15.43N	40.72E	10	4.0	4.05
2	2004/09/03	00:04:12	15.68N	40.70E	5	4.0	4.42
3	2005/04/23	19:11:41	39.46N	16.83E	19	4.1	4.41
4	20005/05/05	13:21:21	41.89N	13.71E	19	3.5	3.41
5	20005/05/21	19:55:19	40.99N	14.51E	16	3.7	3.55
6	2005/10/30	19:09:46	38.53N	15.93E	24	3.6	3.56



In the following there are the results obtained for two of the earthquakes reported in table 2.2; the detail of the inversion procedure are given in (Herrmann R.B. and Ammon C.J. 2002). The tools were used with good traces observed at short distance to determine the focal mechanism, depth and seismic moment. This technique requires a high quality signal and well determined velocity model for the Green functions. To the extent that these are the quality data, this type of mechanism should be preferred over the radiation pattern technique which requires the separate step of defining the pressure and tension quadrants and the correct strike. The observed and predicted traces are filtered using the following frequency bands: 0.02-0.1 Hz

### **SOURCE INVERSION # 1**

#### WAVEFORM INVERSION

The focal mechanism was determined using broadband seismic waveforms. The location of the event and the stations used for the waveform inversion are shown in the next figure.

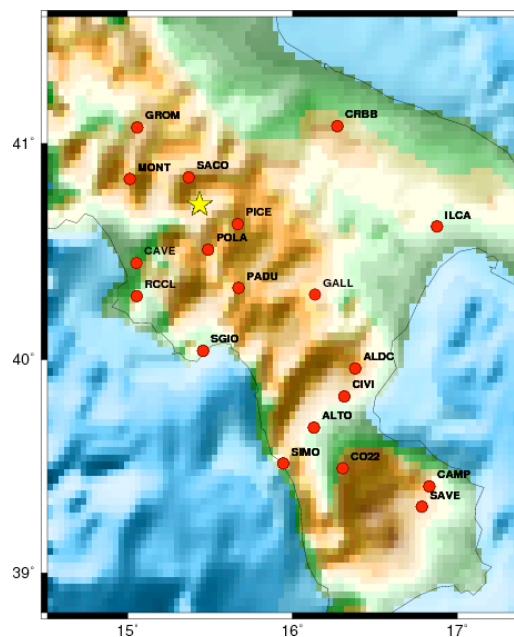


*Figure 2.9: Location of broadband stations used for waveform inversion for the event #1.*





The results of this grid search from 0.5 to 19 km depth are as follow:

	DEPTH	STK	DIP	RAKE	MW	FIT
WVFGRD96	0.5	270	30	100	3.67	0.2731
WVFGRD96	1.0	205	45	30	3.64	0.2690
WVFGRD96	2.0	60	55	90	3.80	0.3456
WVFGRD96	3.0	200	50	20	3.81	0.3689
WVFGRD96	4.0	185	25	0	3.87	0.4239
WVFGRD96	5.0	180	30	-15	3.90	0.4817
WVFGRD96	6.0	180	30	-15	3.92	0.5255
WVFGRD96	7.0	175	35	-25	3.95	0.5586
WVFGRD96	8.0	175	35	-25	3.99	0.5813
WVFGRD96	9.0	175	35	-25	4.01	0.5983
WVFGRD96	10.0	170	35	-35	4.03	0.6075
WVFGRD96	11.0	170	35	-35	4.04	0.6128
WVFGRD96	12.0	170	40	-35	4.05	0.6151
WVFGRD96	13.0	170	40	-30	4.06	0.6124
WVFGRD96	14.0	175	30	-45	4.11	0.6122
WVFGRD96	15.0	175	30	-45	4.11	0.6066
WVFGRD96	16.0	185	35	-35	4.12	0.6031
WVFGRD96	17.0	185	35	-35	4.13	0.5954
WVFGRD96	18.0	180	35	-40	4.14	0.5882
WVFGRD96	19.0	180	35	-40	4.14	0.5889
WVFGRD96	20.0	155	25	-65	4.16	0.5829
WVFGRD96	21.0	160	25	-55	4.21	0.5603
WVFGRD96	22.0	155	25	-60	4.22	0.5509
WVFGRD96	23.0	155	25	-60	4.23	0.5414
WVFGRD96	24.0	160	25	-55	4.24	0.5298
WVFGRD96	25.0	140	25	-70	4.24	0.5178
WVFGRD96	26.0	145	25	-65	4.25	0.5052
WVFGRD96	27.0	140	25	-70	4.25	0.4901
WVFGRD96	28.0	150	25	-60	4.26	0.4746
WVFGRD96	29.0	155	25	-55	4.26	0.4573

The best solution is the one highlighted in the previous table. The mechanism corresponding to the best fit is given in figure 2.10; there are also reported the first motion data. The best fit as a function of depth is given in the figure 2.11.

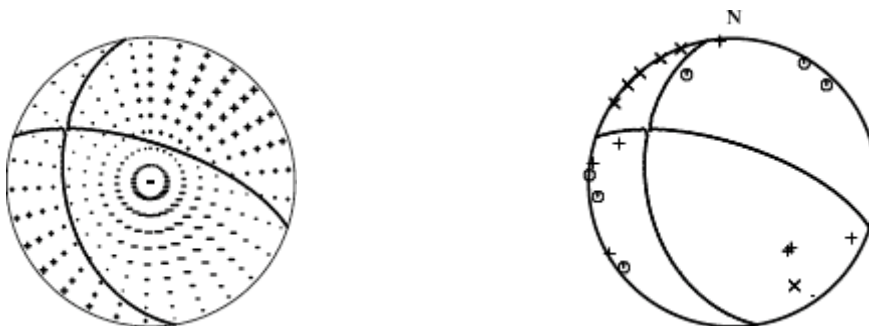
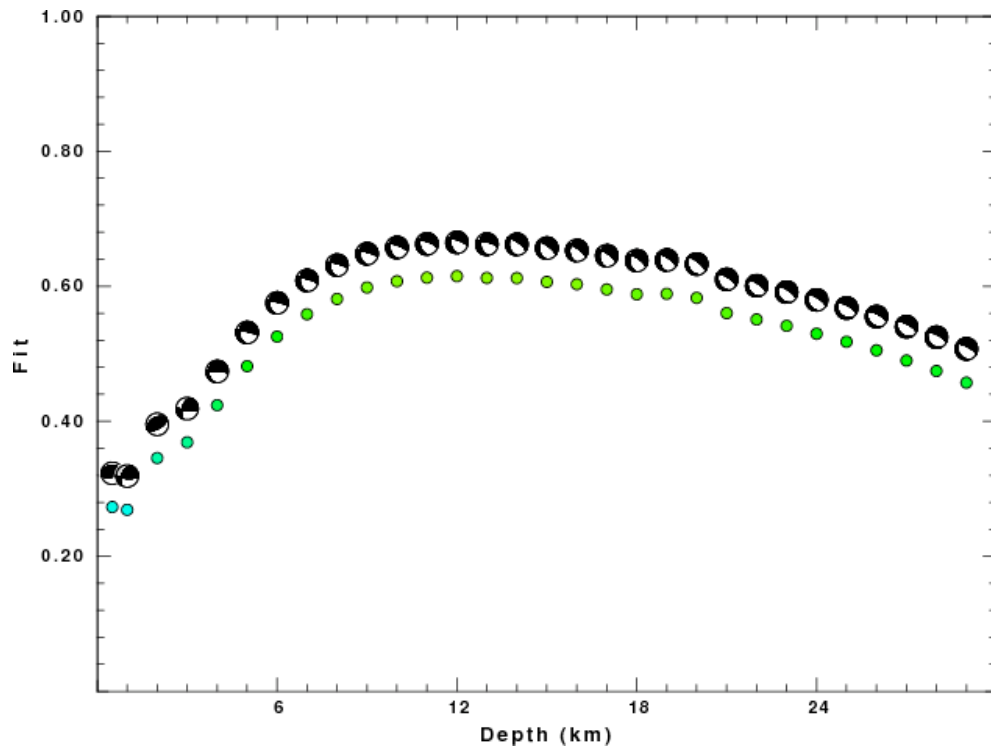
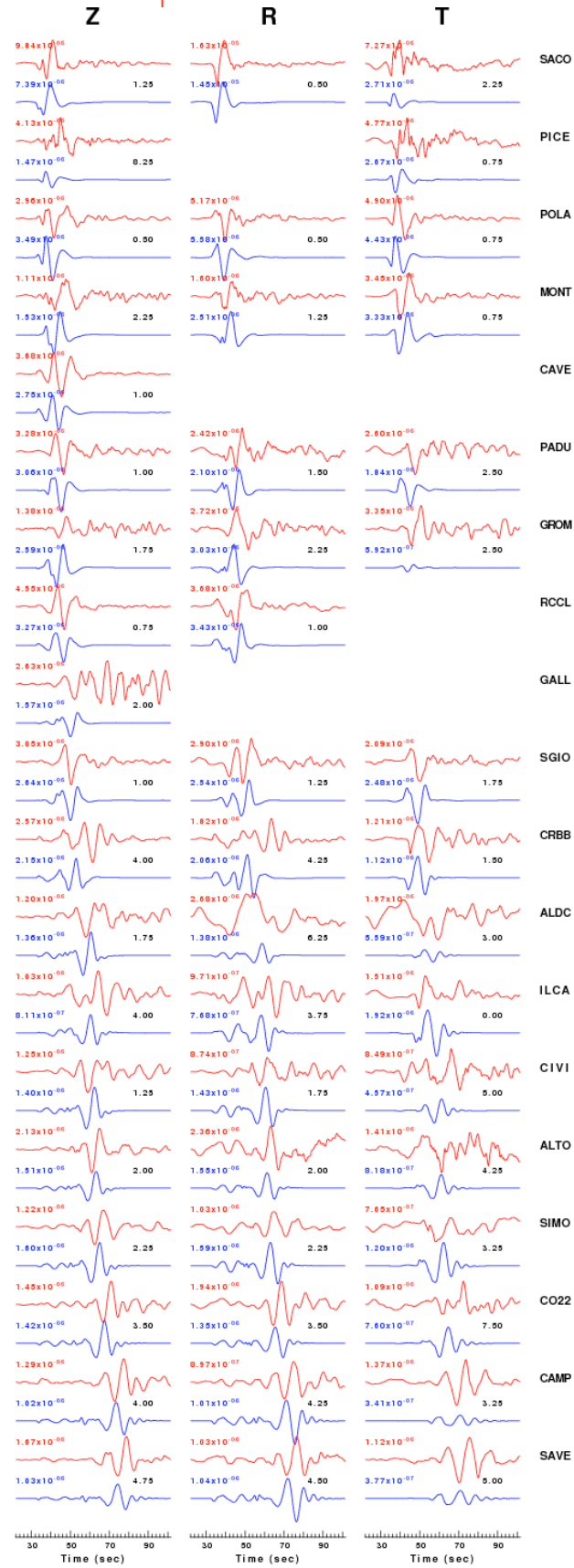


Figure 2.10 Waveform inversion focal mechanism and first motion data



*Figure 2.11: Depth sensitivity for waveform mechanism*

The comparison of the observed and predicted waveforms is given in the next figure. The red traces are the observed and the blue are the predicted. Each observed- predicted component is plotted to the same scale and peak amplitudes are indicated by the numbers to the left of each trace. The number in black at the right of each predicted traces is the time shift required for maximum correlation between the observed and predicted traces. This time shift is required because the synthetics are not computed at exactly the same distance as the observed and because the velocity model used in the predictions may not be perfect. A positive time shift indicates that the prediction is too fast and should be delayed to match the observed trace (shift to the right in this figure). A negative value indicates that the prediction is too slow.





## SOURCE INVERSION # 2

### WAVEFORM INVERSION

The focal mechanism was determined using broadband seismic waveforms. The location of the event and the stations used for the waveform inversion are shown in the next figure.

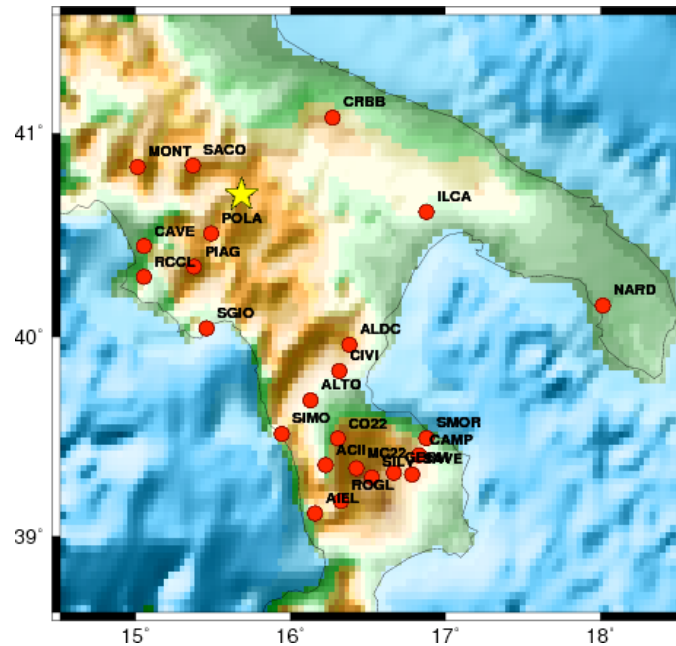


Figure 2.12: Location of broadband stations used for waveform inversion for the event #2.

### FOCAL MECHANISM

#### SLU Moment Tensor Solution

2004/09/03 00:04:12 15.68N 40.70E 5 4.0 Italy

#### Best Fitting Double Couple

$M_0 = 4.79e+22$  dyne-cm

$M_w = 4.42$

$Z = 10$  km

Plane	Strike	Dip	Rake
NP1	190	85	45
NP2	95	45	173

#### Principal Axes:

Axis	Value	Plunge	Azimuth
T	$4.79e+22$	34	63
N	$0.00e+00$	45	195
P	$-4.79e+22$	26	314





WVFGRD96	19.0	185	90	45	4.48	0.4428
WVFGRD96	20.0	185	90	45	4.48	0.4339
WVFGRD96	21.0	0	85	-55	4.53	0.4286
WVFGRD96	22.0	0	85	-50	4.54	0.4181
WVFGRD96	23.0	5	95	-45	4.54	0.4105
WVFGRD96	24.0	185	85	40	4.55	0.4022
WVFGRD96	25.0	185	80	40	4.55	0.3939
WVFGRD96	26.0	185	80	40	4.56	0.3856
WVFGRD96	27.0	185	80	40	4.56	0.3764
WVFGRD96	28.0	185	80	40	4.57	0.3670
WVFGRD96	29.0	190	75	40	4.56	0.3567

The best solution is the one highlighted in the previous table. The mechanism corresponding to the best fit is given in figure 2.13; there are also reported the first motion data. The best fit as a function of depth is given in the figure 2.14.



Figure 2.13 Waveform inversion focal mechanism and first motion data

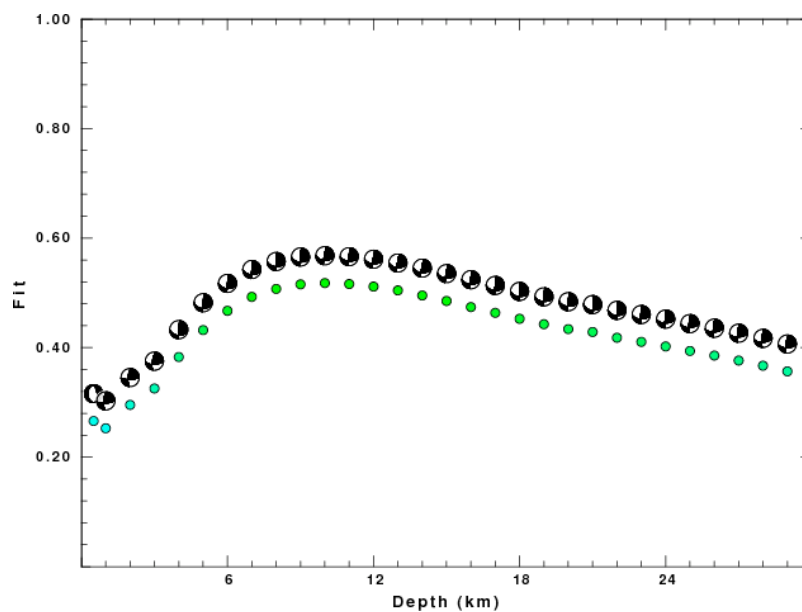


Figure 2.14: Depth sensitivity for waveform mechanism

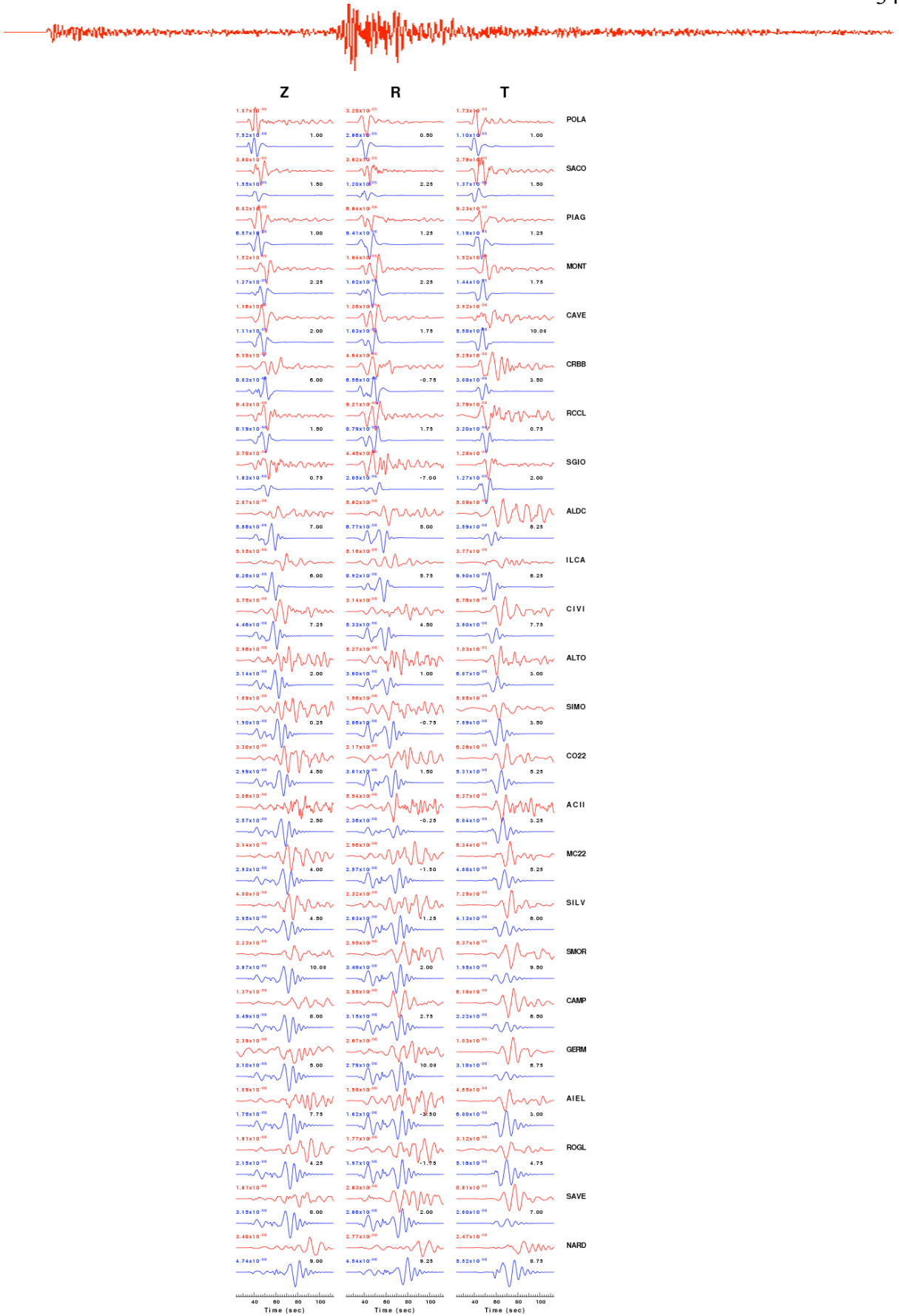
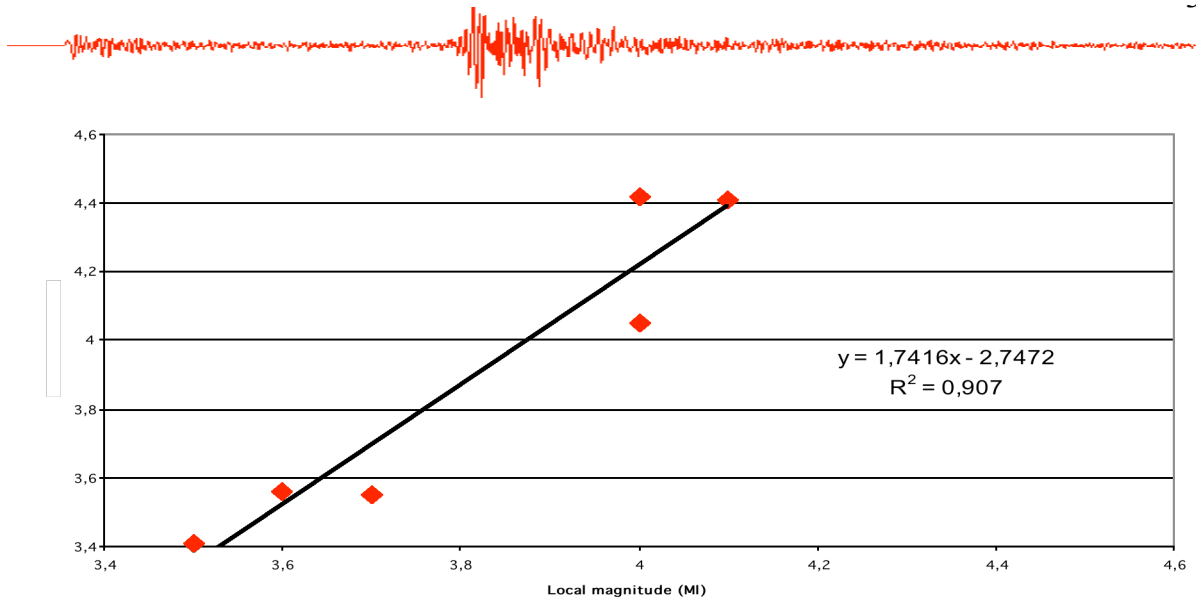


Figure 2.16. Comparison of observed (red) and the predicted (bleu) waveforms.



*Figure 2.17 Local magnitude versus moment magnitud determined in this study*

Figure 2.17 shows the comparison between the given magnitude for the events (MI) versus the magnitude (Mw) obtained by this study. I derived a linear regression in a L2-norm obtaining a linear relation between the given local magnitude (MI) and the obtained moment magnitude (Mw). The correlation coefficient is quite close to 1 indicating a goodness for the fit. However more data will be processed in order to get a more stable relationship.



## **CHAPTER III**

### ***Evaluation of the Regional Scaling Relationships***

#### ***3.1 Methodology***

A possible approach for obtaining regional scaling relationships is to gather a large number of strong-motion recordings and perform regressions on the parameters describing the ground motion. Our approach to the problem is to use seismograms from the background seismicity, with the great advantage that large amounts of data from regional seismic networks become immediately available. A general form for a predictive relationship is the following:

$$\log a(f, r) = EXC(f, r_{ref}) + D(r, r_{ref}) + SITE(f) \quad (3.1)$$

where  $a$  is the peak amplitude of the ground motion carried by direct  $S$  or  $Lg$  waves, recorded at the hypocentral distance  $r$ .  $EXC(f, r_{ref})$  is the contribution of the source to the hypocentral distance  $r_{ref}$ ; this arbitrary reference hypocentral distance is chosen in between the hypocentral distance data set distribution, and large enough to avoid the effect of source depth error in the hypocentral distance. The distance of 40 km satisfies these conditions, and it is the same in similar studies in other regions, so we can compare the results.  $SITE(f)$  is the site term.  $D(r, r_{ref}, f)$  is the crustal propagation term, and represents an estimate of the average crustal response for the region. For representing the distance dependence of observed motion, we approximate the attenuation term as a piece-wise linear function (Anderson and Lei, 1994; Harmsen, 1997). By using (3.1), we are able to arrange all our observations at frequency  $f$  in a large matrix, and simultaneously invert for source, path (attenuation), and site terms. A



separate inversion is performed at each sampling frequency, with a starting model for the attenuation term taken from the results of the coda normalization method.  $D(r, r_{ref}, f)$  contains both the effects of geometrical spreading and anelastic attenuation. A piecewise linear function  $D(r, r_{ref}, f)$  is used for the inversion; following Yazd (1993), we parameterize  $D(r, r_{ref}, f)$  in (3.1) as a piecewise continuous function with  $N_{nodes}$  nodes.

$$\begin{aligned} D(r, r_{ref}, f) &= \sum_{j=1}^{N_{nodes}} L_j(r) D_j(f); \\ D(r = r_{ref}, r_{ref}, f) &= 0 \end{aligned} \quad (3.2)$$

where  $L_j(r)$  is defined as:

$$L_j(r) = \begin{cases} \frac{r - r_{j-1}}{r_j - r_{j-1}} & \text{if } r_{j-1} \leq r \leq r_j \text{ and } j = 2, 3, \dots, n \\ \frac{r_{j+1} - r}{r_{j+1} - r_j} & \text{if } r_j \leq r \leq r_{j+1} \text{ and } j = 1, 2, \dots, n-1 \\ 0 & \text{otherwise} \end{cases} \quad (3.3)$$

$\{D_j(f)\}_{j=1}^{N_{nodes}}$  are node values such that  $D(r, r_{ref}, f) = D_j(f)$ ; the  $N_{nodes}$  coefficients  $D_j(f)$  are determined by the inversion at each sampling frequency. The presence of a large number of nodes in the parameterization of  $D(r, r_{ref}, f)$  guarantees a great flexibility of the empirical attenuation function, allowing a detailed description of the attenuation phenomena. A smoothness constraint can be applied during the inversion to  $D(r, r_{ref}, f)$  by requiring:

$$D_{j-1}(f) - 2D_j(f) + D_{j+1}(f) = 0 \quad (3.4)$$

With an even spatial sampling, the equation above describes a minimum roughness constraint. Throughout this article, the smoothness operator (3.4) is applied in each



regression. After the inversions are run at the set of central frequencies,  $\{f_{0i}\}$ , RVT is used to model the empirical estimate of  $D(r, r_{ref}, f)$ . Duration is an input parameter to RVT, and it must be empirically quantified as a function of hypocentral distance at each sampling frequency. Regressions were carried out separately on peak values of filtered ground velocity and on Fourier spectral amplitudes at the same set of selected central frequencies,  $f$  (see schema in figure 3.1). To obtain the filtered time histories around a target frequency  $f_{0i}$ , we apply a high-pass butterworth (8-pole,  $f_{ci} = f_{0i}/(2)^{1/2}$ ) followed by a low-pass butterworth (8-pole,  $f_{ci} = (2)^{1/2}f_{0i}$ ). The normalized attenuation function (formula 3.x) is used for the forward problem. The geometrical spreading factor  $g(r)$  can be defined on the basis of considerations about the crustal structure of the region of interest: referring to a log–log space, Atkinson (1993) used a trilinear geometrical spreading, whereas other authors (Raouf *et al.*, 1999) required only a bilinear geometrical spreading. The last step in the processing is the modeling of the inverted excitation terms. A source model calibrated on the region is now necessary. For each sampling frequency, absolute amplitudes are propagated to the reference distance using the attenuation relationship just obtained, and the corresponding duration estimated at the reference distance. A term  $\exp(-\pi k_0 f)$  is used to fit the spectral shape of the excitation function at high frequencies. The parameter  $k_0$  is determined in a trial-and-error procedure. Theoretical excitation terms at the reference hypocentral distance are computed at a set of moment magnitudes and compared to the empirical quantities  $\text{EXC}(f, r_{ref})$ . The  $\text{SITE}(f)$  and  $\text{EXC}(f, r_{ref})$  terms defined in (6) are computed in the regression; even though there are more effective methods for investigating these terms, the ones computed here are important to check the stability of the attenuation results. In our computation we do not classify and divide the site terms into specific



groups (i.e., stiff and soft soil sites, rock and hard-rock ones). Instead, we reduce the number of free parameters in the regressions by forcing the function  $D(r, r_{\text{ref}}, f)$  to be zero at the reference distance. This will define an “excitation” term at  $r_{\text{ref}} = 40$  km, rather than a “source” term. Another constraint is obtained by forcing:

$$\sum_i \text{site}(f)_i = 0 \quad (3.5)$$

The constraint (3.5) may strongly influence the excitation terms if a common systematic effect is present at all sites. If this situation occurs, the constraint on the site terms forces the common feature into the source terms during the inversion. The excitation term thus represents the network average expected level of motion at the reference distance.

## ***3.2 Results***

### ***Duration of Ground Motion***

To quantify the different parameters characterizing the ground motion in the region we used the Random Vibration Theory (RVT; Cartwright and Lougnet-Higgins, 1956). Duration of ground-motion is, in general, a function of fault size and of the dispersion of elastic waves along the path between the source and the seismic station (Herrmann, 1975, 1985?; Boore, 1986). Our definition of effective duration of ground-motion is the same of that given by (Raouf et al. 1999). For each seismogram the duration  $T$  is determined and its definition is given as the width of the time window that limits the 5%-75% portion of the seismic energy following the S-wave arrivals. In the figure the duration for all the recordings available are reported.

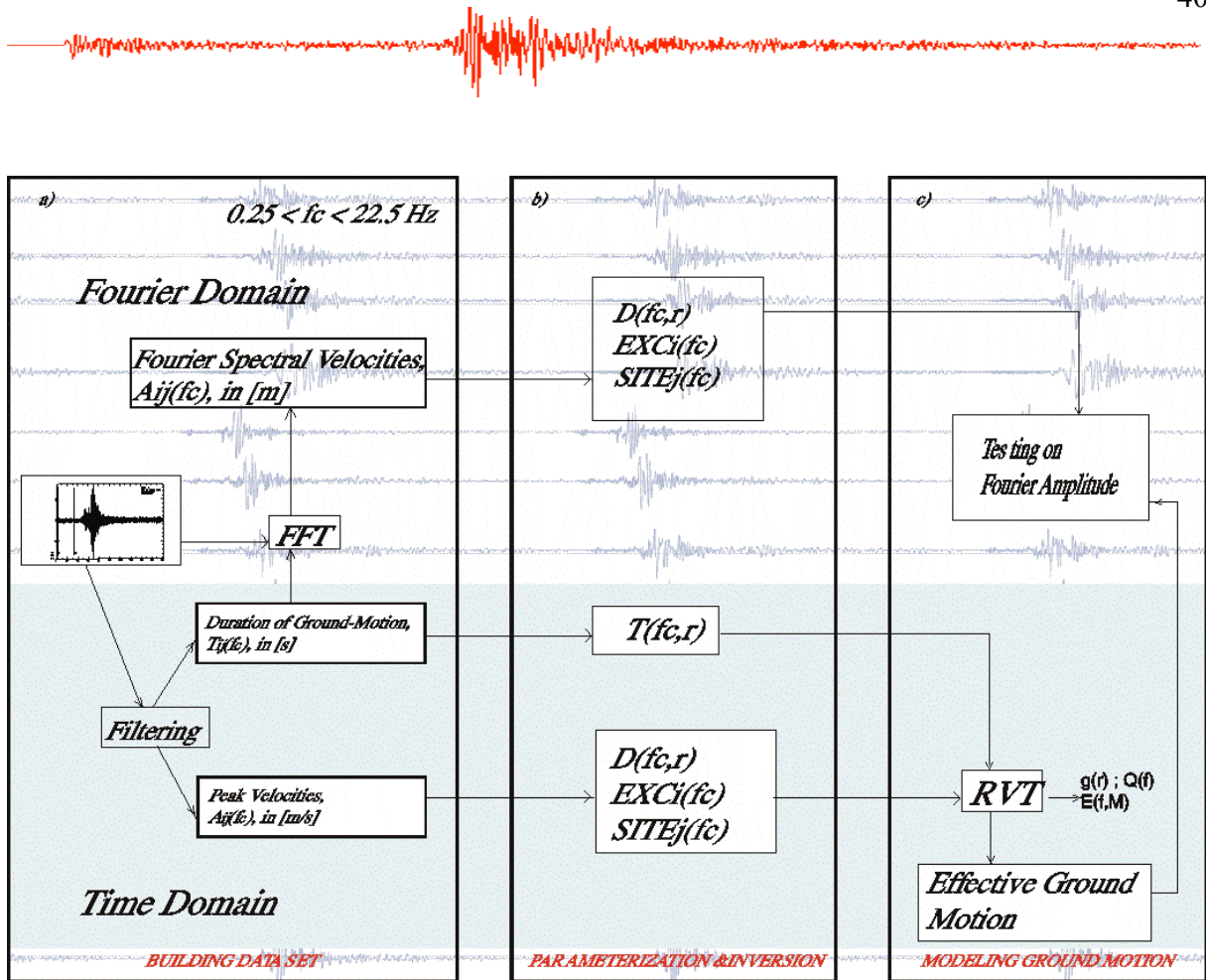


Figure 3.1 : Schematic approach of the methodology used

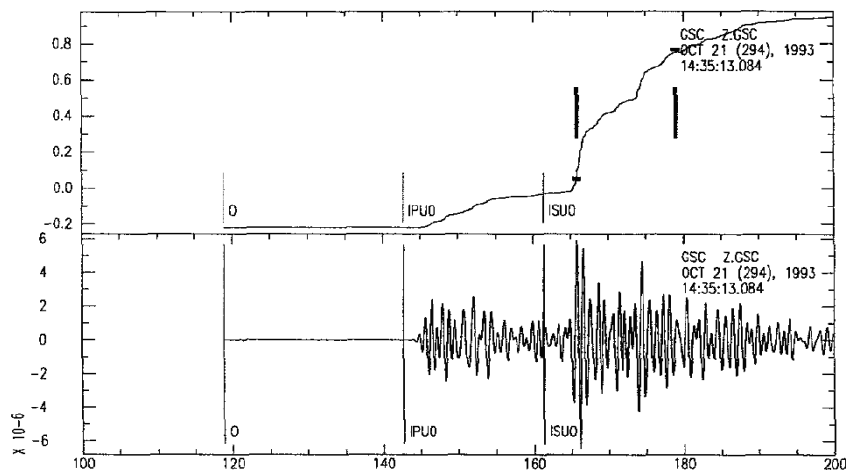


Figure 3.2: Illustration of method of estimating duration. The lower trace is the velocity time history filtered at 1.0 Hz. The upper trace is the integrated square velocity. The duration of 14 sec is the time interval between the 0.05 and 0.75 ordinate. The origin and P and S arrival times (IPU0 and ISU0, respectively) from the unfiltered time history are indicated. The group delay of the filter is apparent by the shift of the P and S arrivals from the picked time.

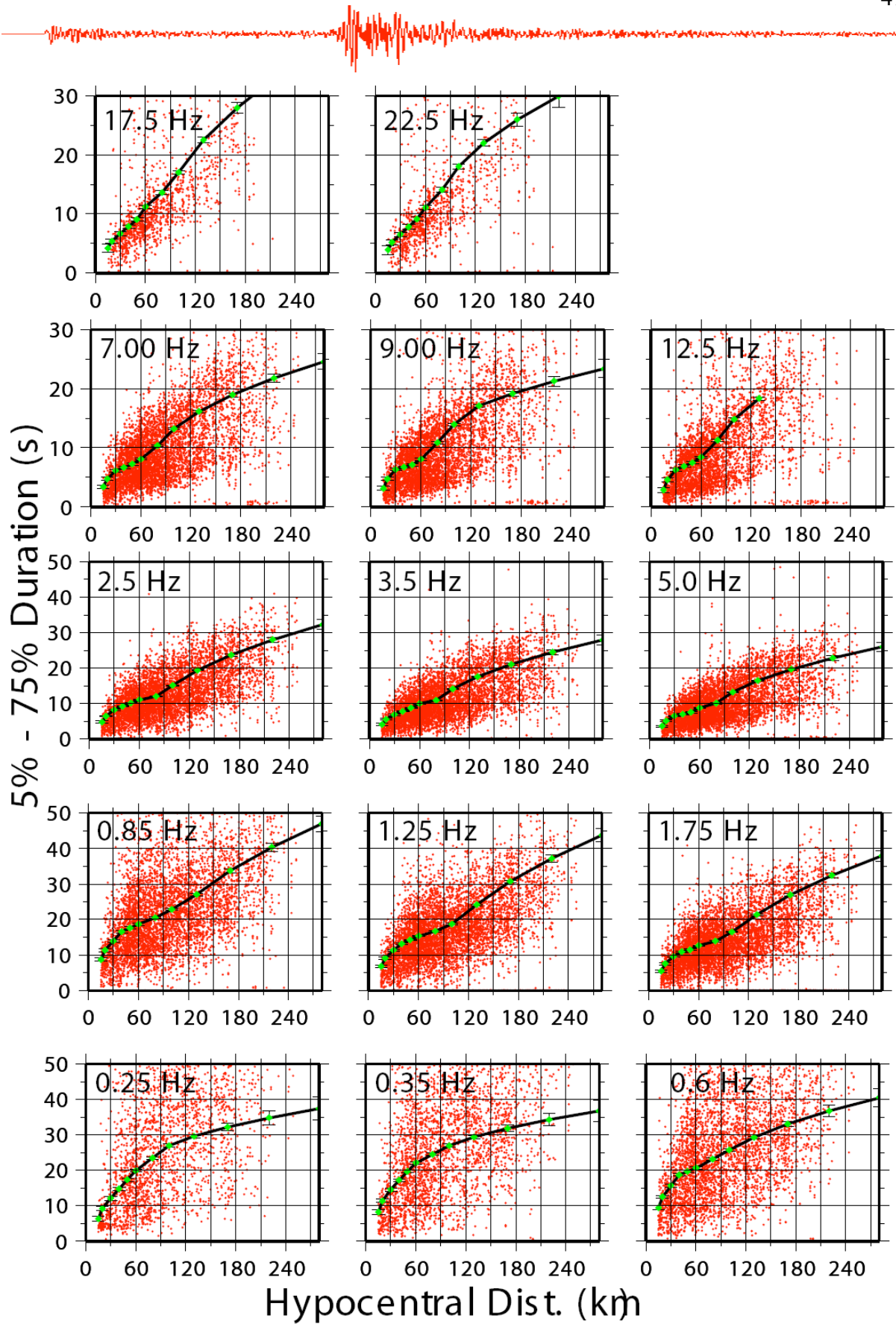


Figure 3.3: Duration of the seismic signals and associated standard errors as a function of hypocentral distances for each frequency studied. A linear interpolation scheme is used in the regressions for intermediate distances.



### ***Regional Attenuation***

In this section we show the results of the regression at a set of sampling frequencies.

The empirical attenuation is modeled by using the following functional form:

$$D(r, r_{ref}, f) = \log[g(r)] - \log[g(r_{ref})] - \frac{\pi f (r - r_{ref})}{\beta Q(f)} \quad (3.6)$$

where  $g(r)$  is called geometrical spreading. It can be defined on the basis of consideration about the crustal structure of the region of interest;  $\beta$  is the shear-wave velocity (3.5Km/sec) and

$$Q(f) = Q_0 \left( \frac{f}{f_{ref}} \right)^\eta \quad (3.7)$$

The color curves in figure 4 represent the empirical propagation term at different central frequencies, while the black lines represent the theoretical predictions obtained after a trial-and-error modeling of empirical curves. In this paper we suggest a model having  $Q_0=190$ ,  $\eta=0.65$  and  $f_{ref}=1.0\text{Hz}$ , so the equation (4) becomes

$$Q(f) = 190(f)^{0.65} \quad (3.8)$$

and a geometrical spreading of:

$$g(r) = \begin{cases} r^{-1.0} & 1 < r < 100\text{km} \\ r^{-0.5} & r > 100\text{km} \end{cases} \quad (3.9)$$

As shown in figure 4 the attenuation term was forced to zero at the reference distance of 40 km.

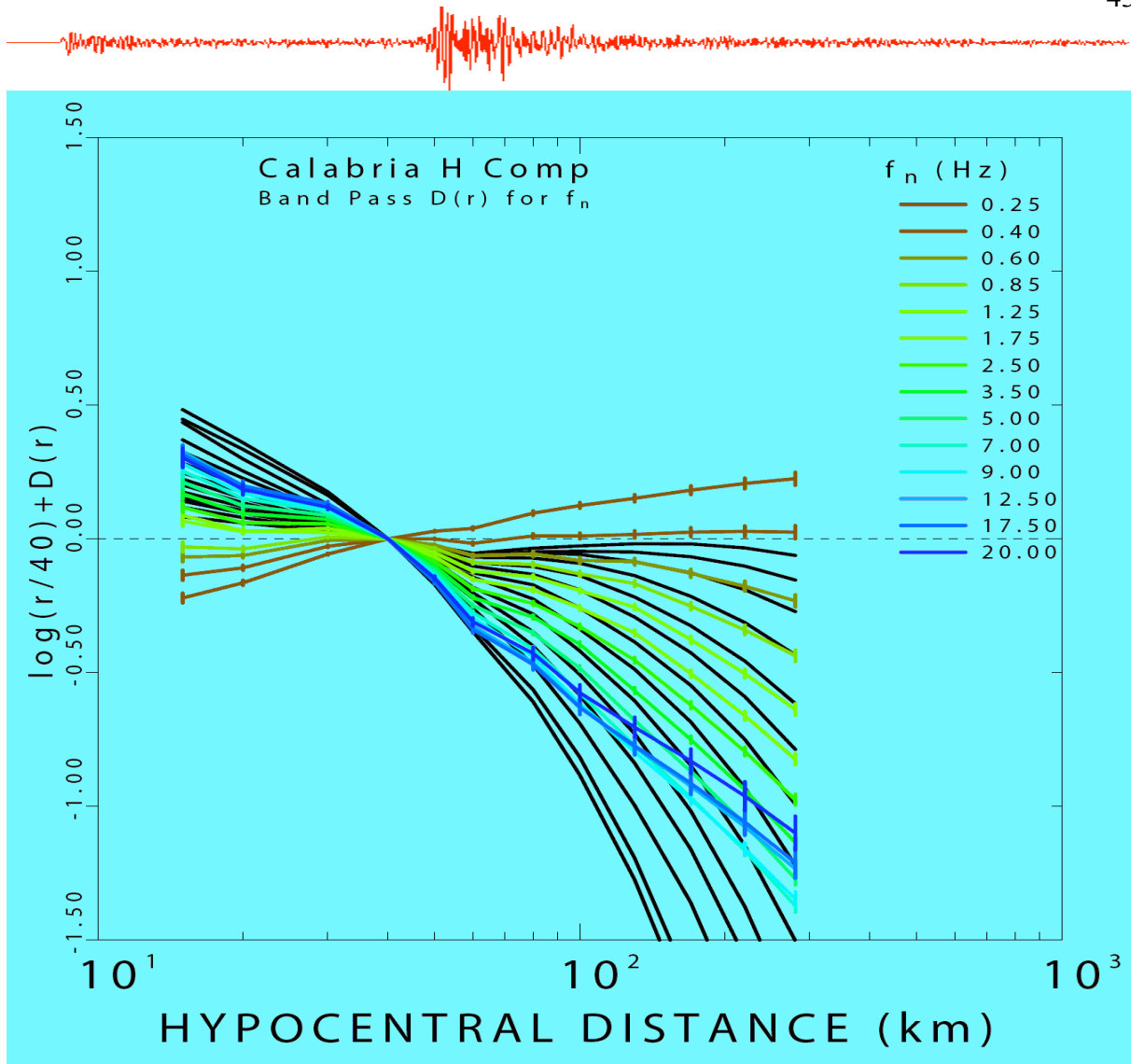
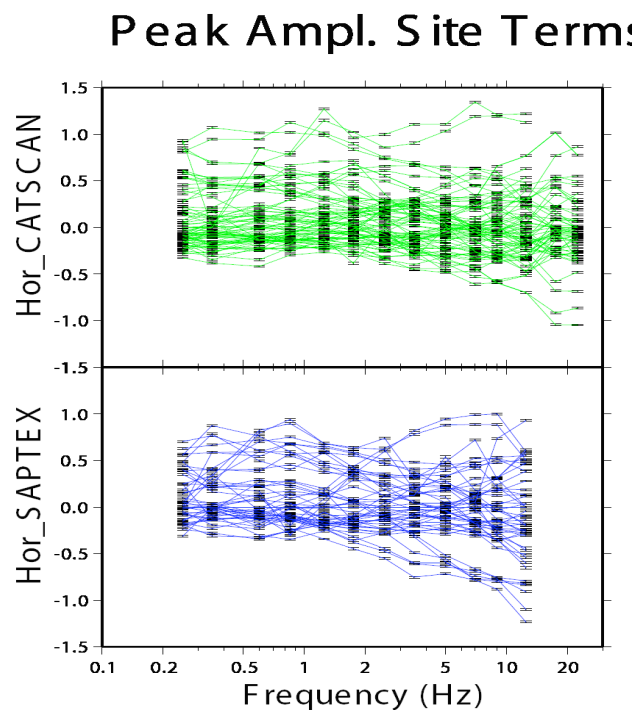


Figure 3.4: Colored curves are the empirical propagation term at the central frequencies of 0.25, 0.40, 0.60, 0.85, 1.25, 1.75, 2.50, 3.50, 5.00, 7.00, 9.00, 12.50, 17.50, 20.00 Hz, resulting from the regression of the peak value of the data set waveforms. The attenuation term was forced to be zero at the reference distance of 40 km. Black lines are our theoretical predictions, which were obtained for each central frequency through the use of RVT.



### *Site Term*

During the inversion the sum of all site terms is forced to zero (relation 2a) for each frequency. This constraint represents what would be recorded at the reference hypocentral distance by the average network site. The site term measures the deviation from the mean seismic spectra for each station, which is due to the physical properties of the shallow geology at the recording site. In figure 5 the site term for each central frequency is plotted. The figure verifies the accuracy of the instrument calibration. At this stage we took in account just the rock site according the classification given in the table 2.1 in the previous chapter.



*Figure 3.5: Site term from the regression of the data set*



### ***Excitation Term***

In the relation 1 the term  $EXC(f, r_{ref})$  represents the ground motion excitation at the Earth's surface at the reference distance. It depends on source characteristic such as the energy released and it is valid for the average site class. The excitation terms are modeled by using the following functional form:

$$exc(f, r_{ref}) = C(2\pi f)M_0 s(f)g(r_{ref}) \exp\left[-\frac{\pi r_{ref}}{\beta Q(f)}\right] v(f) \exp(-\pi f k_0) \quad (3.10)$$

including the crustal attenuation,  $Q(f)$ , the geometrical spreading  $g(r=r_{ref})$ ; the parameter  $k_0$  and the generic rock site amplification  $v(f)$ , like the one used by Atkinson and Silva (1997).

$$s(f) = \frac{1}{1 + \left(\frac{f}{f_a}\right)^2} \quad (3.11)$$

and being

$$C = \frac{RVF}{4\pi\rho\beta^3} \quad (3.12)$$

*Table 3.1 High-Frequency Ground-Motion parameters*

$$C = RVF/4\pi\rho\beta^3$$

$$R=0.80; V=0.707 F=2.0 \rho=2.8g/cm^3; \beta=3.5km/s$$

$$S(f) = 1/[1 + (f/f_a)^2]$$

$$f_a = 4.9 \cdot 10^6 \beta (\Delta\sigma/M_0)^{1/3} \text{ Hz}$$

$$\Delta\sigma = 250 \text{ bar } K_0 = 0.040s \quad V(f) = 1.0$$

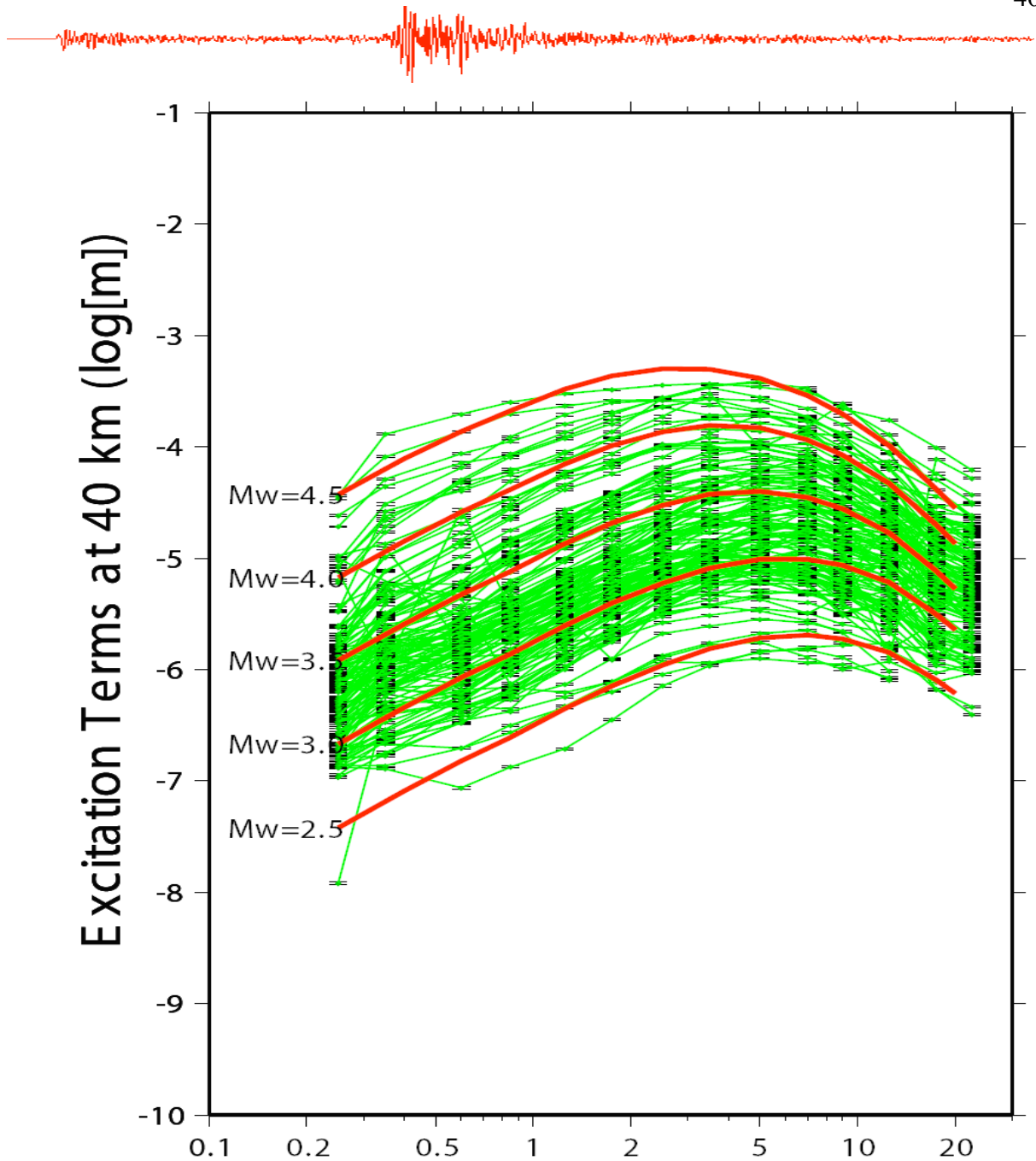


Figure 3.6: Estimated excitation terms of the peak-filtered velocity at the reference distance of 40 km. Red lines are the theoretical prediction performed using the RVT and the source parameters in table 3.1. Green lines are the observed data. The plot is given for the CAT-SCAN experiment

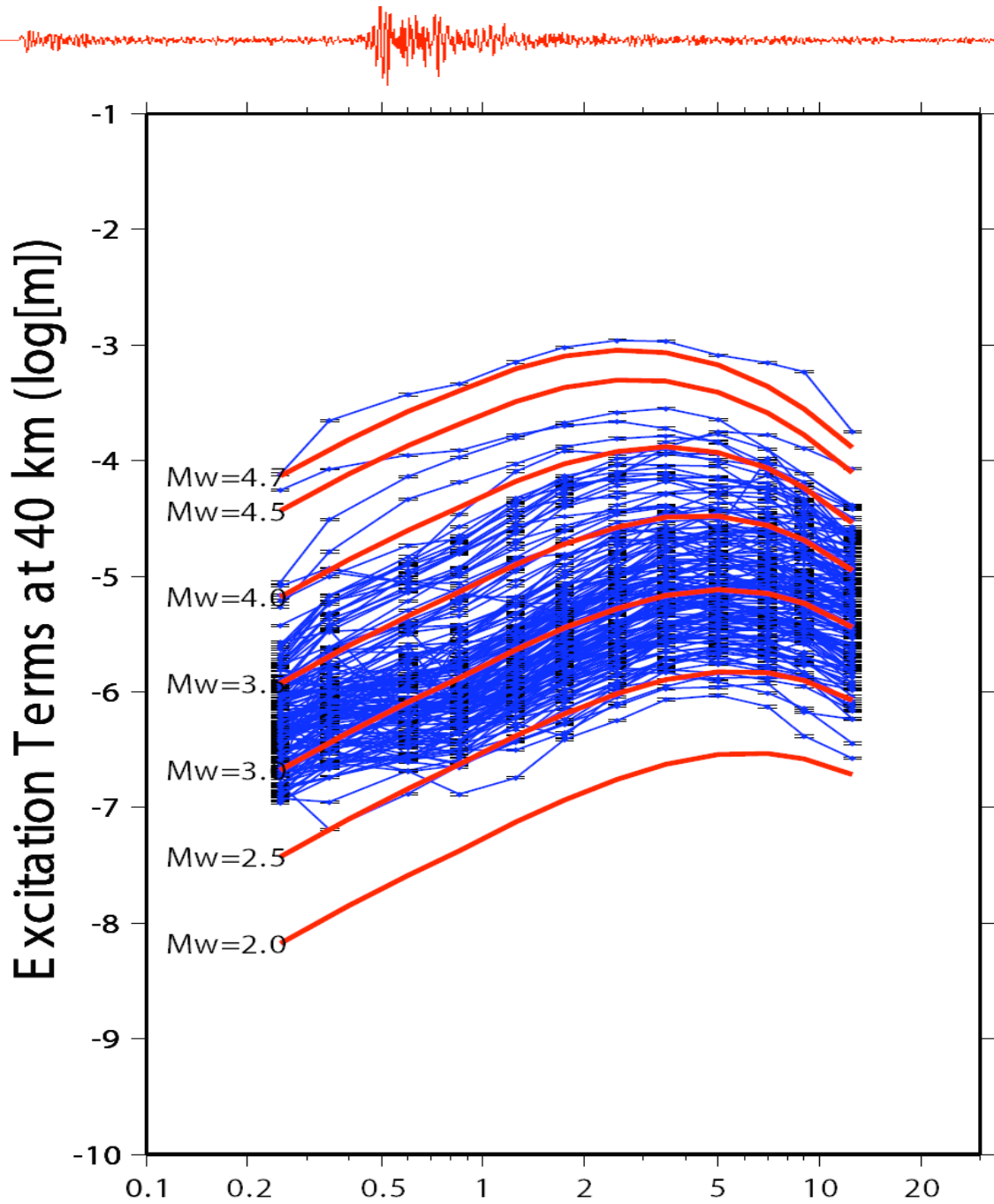
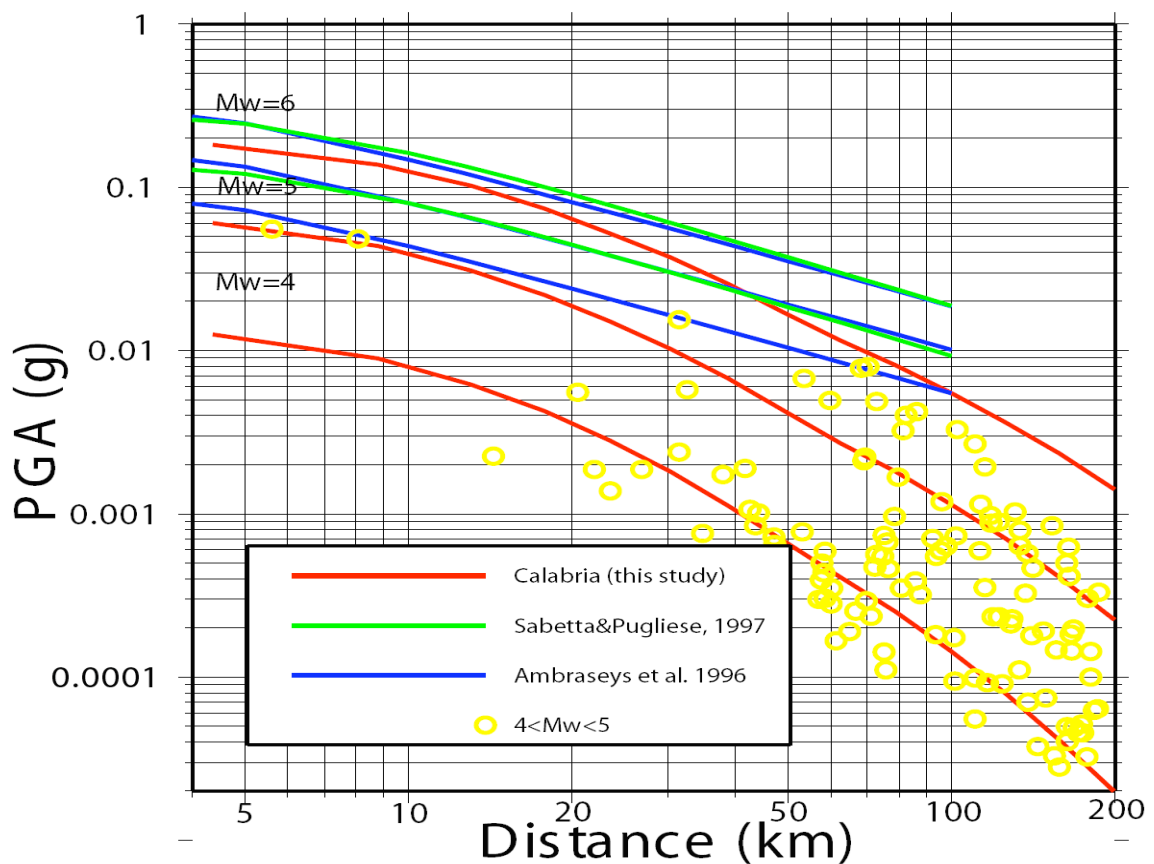


Figure 3.7: Estimated excitation terms of the peak-filtered velocity at the reference distance of 40 km. Red lines are the theoretical prediction performed using the RVT and the source parameters in table 3.1. Blue lines are the observed data. The plot is given for the SAPTEX experiment



### ***Predicted Ground Motion***

Using the source and attenuation parameters computed in this study and a set of programs (SMSIM; Boore, 1996) we predicted the expected Peak Ground Acceleration (PGA). The figure 3.8 shows the comparison for magnitude 4.0, 5.0 and 6.0 among the attenuation relations evaluated in this study and the relationships developed by Ambraseys et al. (1996) for Mediterranean region and Sabetta & Pugliese (1996) for Italy .



*Figure 3.8: Estimation of Peak Ground Acceleration (PGA). Results (red lines) are for this study (derived by using parameters in table 3.1 and estimated attenuation parameters) as a function of distance and for difference values of moment magnitudes. Blue and green lines are results obtained by previous studies while circles represents observed data.*



In the figure 3.8 the Sabetta and Pugliese (1997) and the Abraseys et al. (1996) attenuation relationships are stopped at 100 km because they are calibrated until these distances. It is possible also to notice that the Sabetta and Pugliese (1997) is not plotted for magnitude less than five. For our data set it is also evident that the Sabetta and Pugliese (1997) and the Abraseys et al. (1996) attenuation relationships are not useful. In fact they are calibrated on large events and do not consider the ground shaking due to the intermediate magnitudes. The plot shows also the good agreements between the simulation, using the parameter obtained within this study, and the observed PGA values.



## ***CHAPTER IV***

### ***An Attenuation Relationship for Southern Italy***

#### ***4.1 Introduction: Estimation of Ground Motion***

Since southern Italy is a seismically active region it is really important to define an attenuation relation for the area and because of increasing exposure and vulnerability to the effects of earthquakes, seismic hazard assessment is very important issue in the region. The estimation of ground motion for a particular region and also site-specific investigation is essential for the design of engineered structures. Seismic hazard assessment requires a strong motion attenuation relationship (Kramer, 1996) to estimate ground motions from specific parameters characterizing the nature of earthquake source, the distortion effect of the shallow geology and the effects of the transmitting medium on the seismic waves. A number of such relationships have been developed for many regions of the world (Ambraseys et al., 1996; Boore and Joyner, 1991; Toro and McGuire, 1987; Atkinson and Boore, 1995; Campell, 1997; Sadigh, 1997), mainly by regressing strong-motion data. These studies have shown that the ground motion levels can differ significantly in different tectonic regimes, for example depending on whether stresses are extensional or compressional. In this study we described predictive relationships for the ground motion in the studied area by regressing the peak ground acceleration (PGA) from our data. We employ two-stage regression procedure (Joyner and Boore, 1981, 1993; Ambraseys et al., 1996; Boore et al., 1997) to obtain PGA. Estimates of expected ground motion at a given distance from an earthquake of a given magnitude are fundamental inputs to earthquake hazard



assessments. The determination of seismic design criteria for engineered structures depends upon reproducible estimates of the expected lifetime of the structures. Usually are the so called attenuation relationships that provide these estimates; they are equations given as function of magnitude, distance and other parameters such as type of faulting or type of soil. The parameters that must be clearly defined in order to estimate ground motion are: earthquake magnitude, type of faulting, local site conditions (usually the description of the soil where the receiver is located) and distance. Usually moment magnitude is the preferred measure because it is directly related to the seismic moment of the earthquake. Style of faulting is also an important parameter considered in most attenuation relationships because different mechanisms tend to generate different PGA and high-frequency spectra acceleration (SA) values; for example it is known that thrust earthquakes tend to generate larger PGA and SA than strike-slip or normal faulting. Different researcher use different “source to site” distance measures (figure 4.1). For instance  $r_{jb}$  (the Boore and Joyner distance) is the closest horizontal distance to the vertical projection of the rupture;  $r_{rup}$  is the closest distance to the rupture surface;  $r_{seis}$  represents the closest distance to the seismogenic rupture surface (Marone and Scholz, 1998);  $r_{epi}$  and  $r_{hypo}$  are the epicentral and the hypocentral distance respectively. There are also several site classification schemes used in different papers ranging from qualitative description of the near surface material to very quantitative definitions based on shear wave velocities. Different tectonic environments give rise to different ground motion attenuation relationship. Regardless of the tectonic regime, rupture directivity also may affect ground motion attenuation relationship (Somerville et al., 1997). For larger events, a special problem arises, at short distances, with the source-to-site distance measure, because distance



metrics based on a point-source model are no longer appropriate. As a consequence, different attenuation relations differ in the distance metric that they use. In addition to being a source of confusion, this causes problems to quantitatively compare or combine different ground-motion models. For this reasons, Scherbaum et al. (2004) used well established scaling laws to determine explicit distance conversion relations using regression analysis on simulated data. They demonstrate that, for all practical purposes, most popular distance metrics can be related to the Joyner-Boore distance using models based on gamma distributions to express the shape of some “residual function.”

## 4.2 Methodology

We fit strong-motion data by multiple linear regressions using the equation (modified after Joyner and Boore, 1981 and Ambraseys et al., 1996):

$$\log y = \sum_{i=1}^N a_i E_i + br + c \log r + dS + \varepsilon \quad (4.1)$$

where:

$E_i = 1$  for earthquake  $i$

$E_i = 0$  otherwise

$S = 1$  for soft soil sites

$S = 0$  for stiff soil sites

$r = (d^2 + h^2)^{1/2}$

$\varepsilon =$  residuals



and  $y$  is peak horizontal acceleration,  $N$  is the number of earthquakes in the data sample, and  $d$  is the closest horizontal distance site to the vertical projection of the fault rupture. Values  $a_i$ ,  $b$  and  $c$  are coefficients determined by the first linear regression for a chosen value of  $h$ , and  $h$  is determined by a simple grid-search procedure to minimize the sum of squares of the residuals. Since, our data set has not got stations located on hard rock site, we obtained the coefficients only for stiff and soft soil sites. In this equation,  $\varepsilon = \sigma P$ ;  $\sigma$  is the standard deviation of the residuals. The value of  $P$  is based on the assumption that the prediction errors are normally distributed and  $P=0.84$  confidence level for  $\pm 1\sigma$  values. By using  $E_i$  and  $S$ , we divided the data into classes, this is a well-known technique in regression analysis (Draper and Smith, 1966; Weisberg, 1980; Joyner and Boore, 1981; Boore et al., 1997). The procedure decouples the determination of magnitude dependence from the determination of distance dependence. If the regression analysis were done in terms of magnitude and distance simultaneously, errors in measuring magnitude would affect the distance coefficients obtained from the regression. In this approach, each earthquake has the same weight in determining magnitude dependence and each recording has the same weight in determining distance dependence (Joyner and Boore, 1981). The coefficient,  $h$ , is sometimes referred to as a “fictitious” depth measure (Boore et al., 1997) implying that interpretation of  $h$  is not clear and its value is estimated as part of the regression. Abrahamson and Silva (1997) have reported that  $h$  yields a marginally better fit to the data at short distances. In this study, the distance measure,  $d$ , is the closest horizontal distance to the vertical projection of the rupture. In case that we could not described to rupture surface, especially for small earthquakes,



we used epicentral distance instead of this measure. The parameter  $h$  is introduced to allow for the fact that the source point may not be the closest point on the rupture. In fact, the value obtained for  $h$  incorporates all the factors that tend to limit or reduce motion near the source, including any tendency for the peak horizontal acceleration to be limited by the finite strength of near-surface materials. The value of  $h$  also incorporates any factors that tend to enhance the motion near the source, especially, directivity effect (Joyner and Boore, 1981). After the  $a_i$  values are obtained by the first linear regression, they were used to find, by least squares, a first or second order polynomial representing the magnitude dependence:

$$a_i = \alpha + \beta M_i + \gamma M_i^2 \quad (4.2)$$

Here,  $M$  is moment magnitude  $\alpha$ ,  $\beta$ , and  $\gamma$  are the coefficients determined by the second linear regression. The source of our data set, has got local magnitude rather than moment magnitude so we used the approach given by Malagnini et al. (2000) to compute it.

To estimate  $\sigma$ , the total standard error after two regressions, we assumed that magnitude and distance parameters have not got any correlation between each other.

By using convergence theorem, we can write following equation:

$$\sigma = \sqrt{\sigma_1^2 + \sigma_2^2} \quad (4.3)$$

Where,  $\sigma_1$  is the standard deviation of the residuals from the regression described by equation (4.1) and  $\sigma_2$  is the standard deviation of the residuals from the regression described by equation (4.2).



### 4.3 Results

In the following there are reported the results of the regression and finally it is presented a relationship derived for the southern Italy.

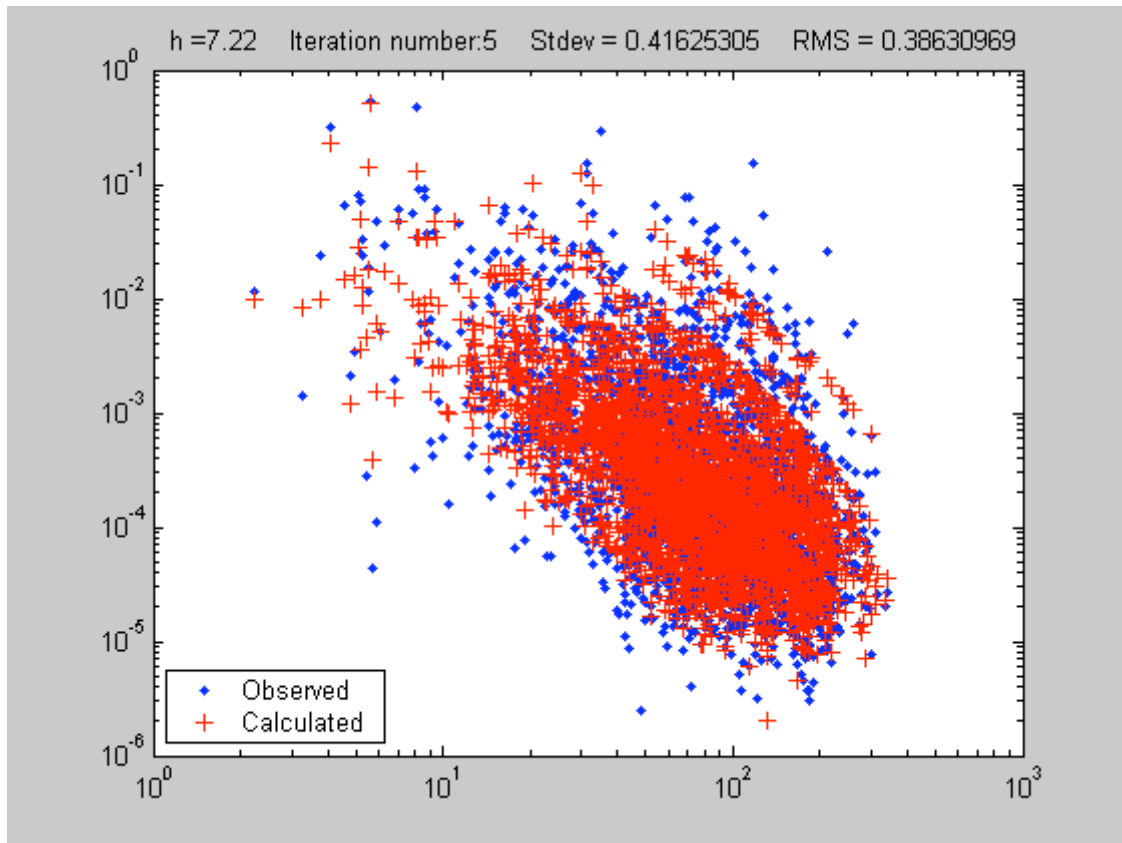


Figure 4.1. Comparison between the observed and predicted data

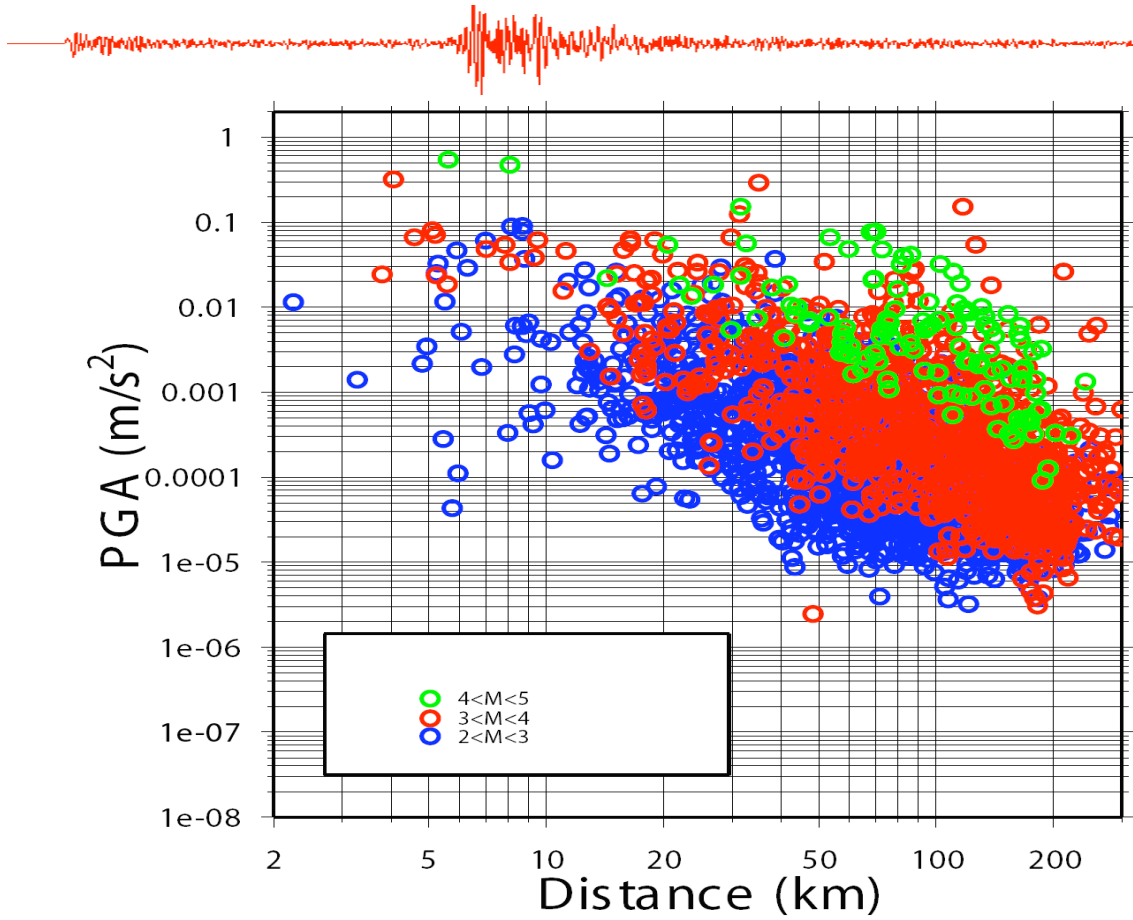


Figure 4.2: Distribution of PGA values versus the distance; different colors denote different range of magnitude

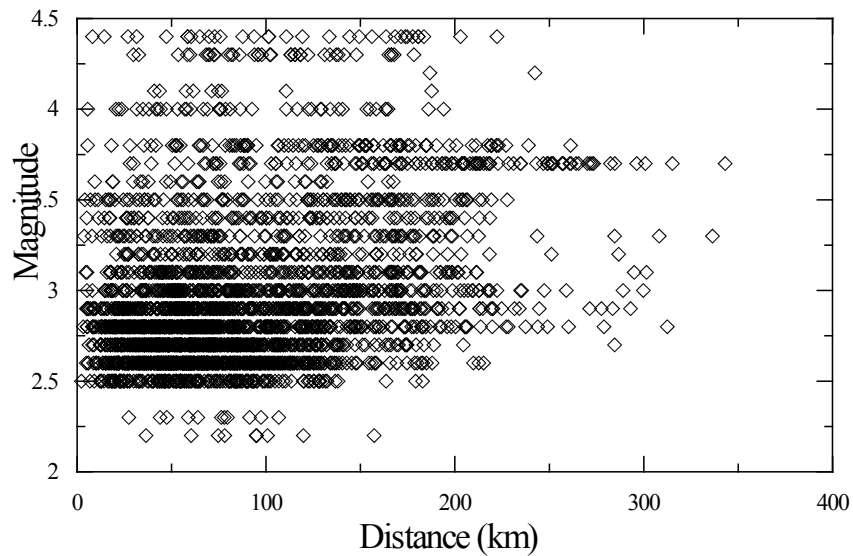


Figure 4.3: Distribution in  $M$  and  $d$  of the data set for peak horizontal acceleration.

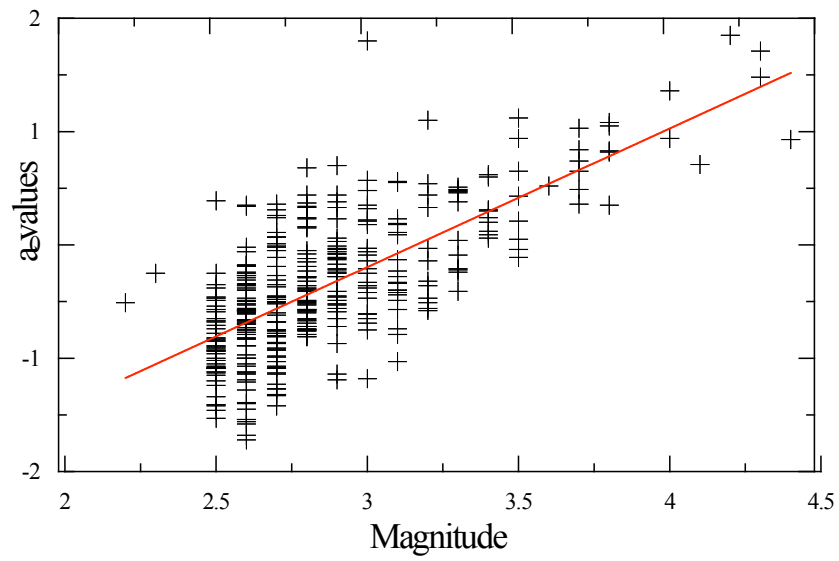


Figure 4.4: Values of  $a_i$  for peak horizontal acceleration from the regression analysis of equation 4.1 plotted versus magnitude.

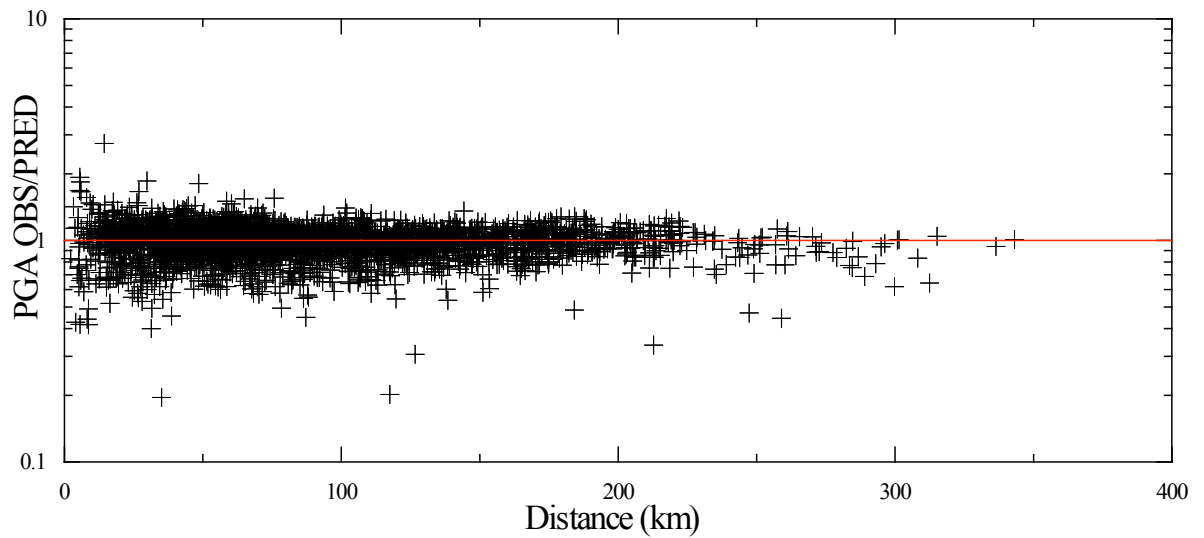


Figure 4.5: Ratio of observed and predicted peak horizontal acceleration versus the distance.

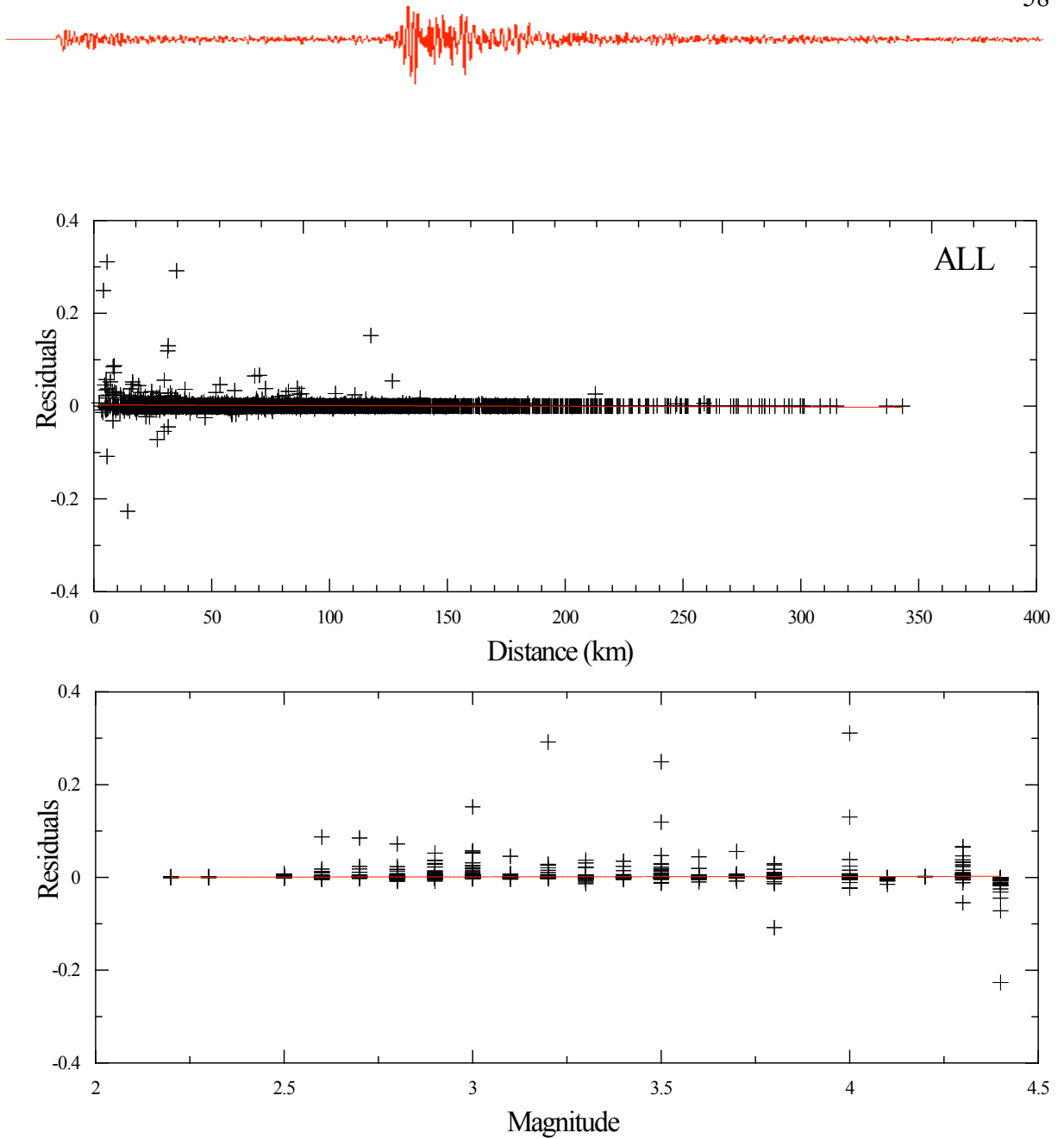


Figure 4.6: Regression of the residuals of peak horizontal acceleration versus the distance and magnitude for all data.

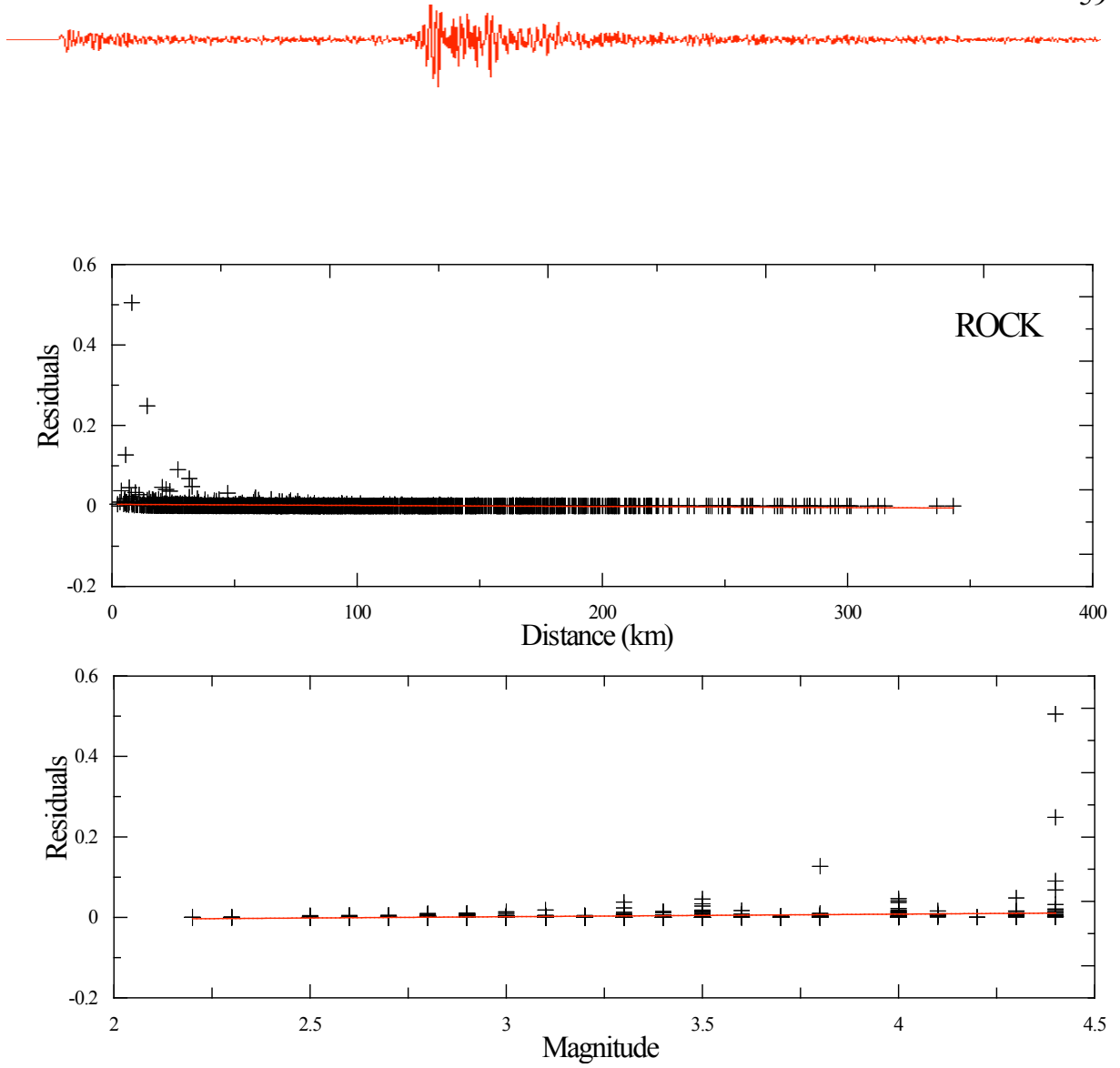


Figure 4.7: Regression of the residuals of peak horizontal acceleration versus the distance and magnitude for rock site.

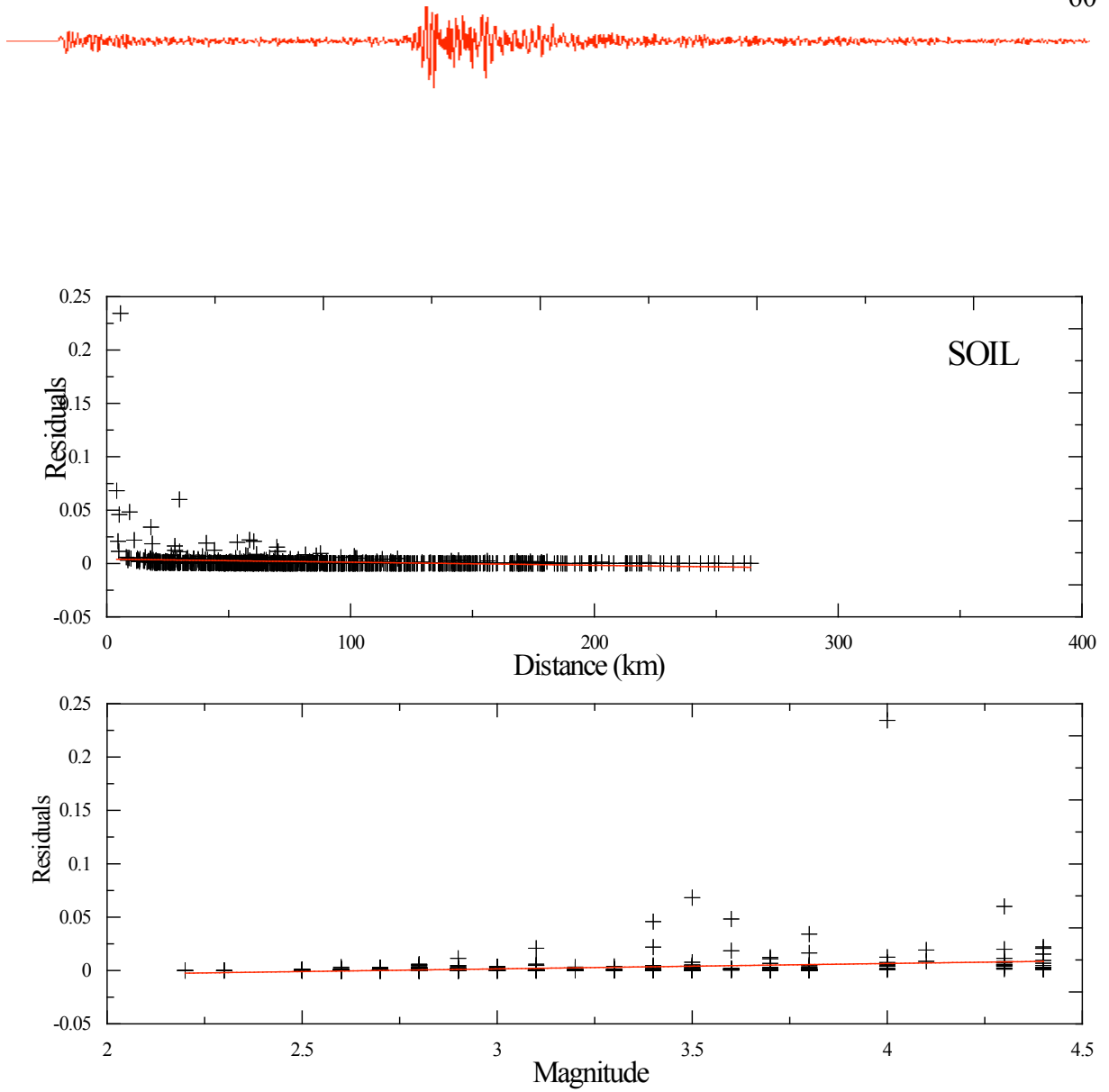


Figure 4.8: Regression of the residuals of peak horizontal acceleration versus the distance and magnitude for stiff soil site.



We obtained for the following functional for the coefficients reported below. Figure 4.9 shows an example for  $M=4$  using the coefficient obtained from the regression.

$$\log y = \sum_{i=1}^n a_i E_i + br + c \log r + dS + \varepsilon$$

$$S = \begin{cases} = 1 & \text{for soft soil sites} \\ = 0 & \text{for stiff soil sites} \end{cases}$$

$$\alpha = -3.87$$

$$\beta = 1.22$$

$$b = 0.0024$$

$$c = -1.727$$

$$d = 0.024$$

The figure shows the predicted peak ground acceleration as a function of distance for an earthquake having magnitude equal to four (blue line); the two red lines represent the “one standard deviation”. The circles are the observed PGA values coming from the events having  $M=4$  present in our data set. It is possible to notice that some of the observed data are out of the “standard deviation limits”, this is due to the possible site effect that tend to amplify the peak ground acceleration at certain sites.

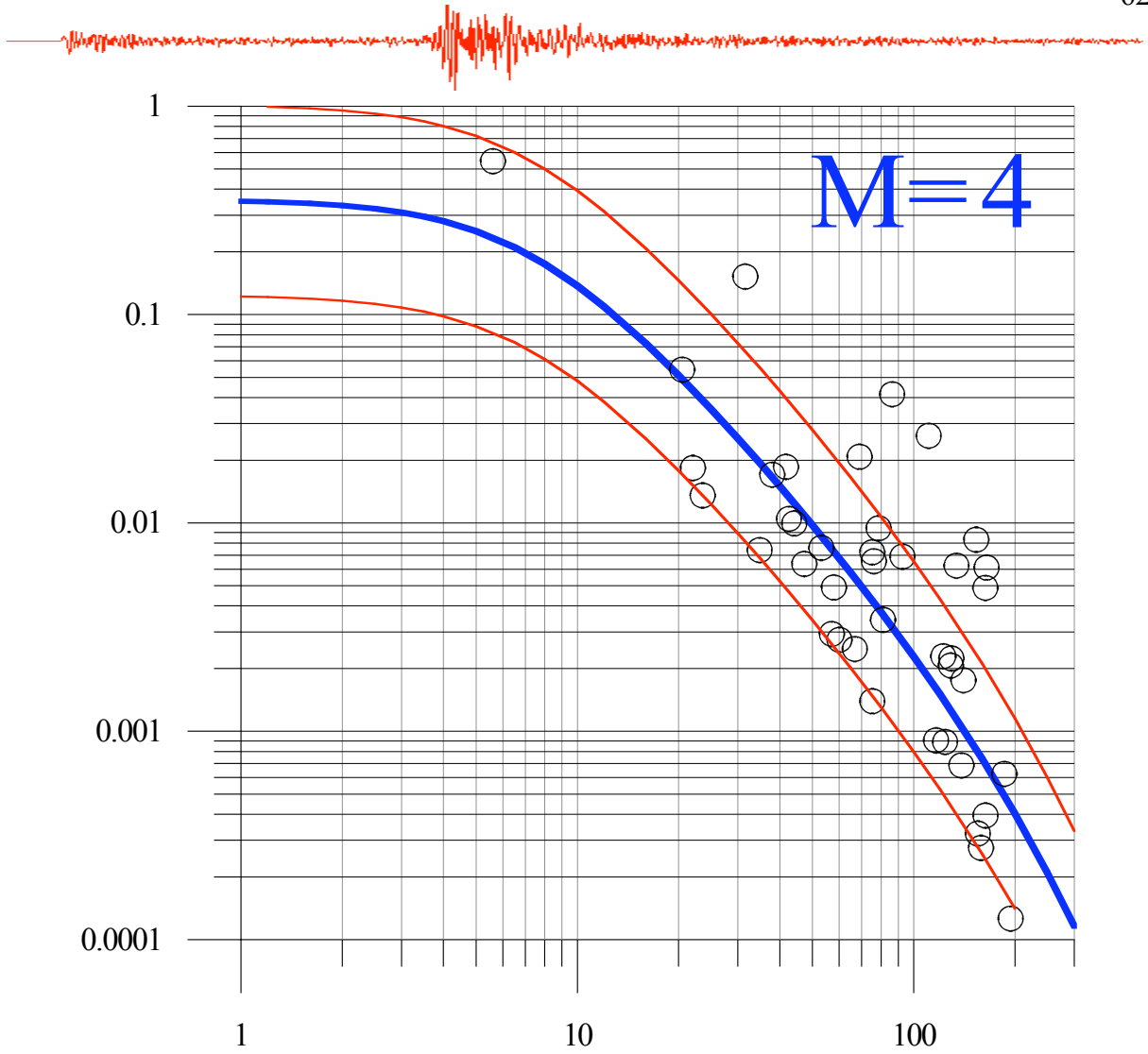


Figure 4.9: Predicted PGA values for  $M=4.0$  event (blue line) and  $\pm 1\sigma$  values (red lines). Observed PGA values for  $M=4.0$  events (circles).



## ***CHAPTER V***

### ***Conclusion***

I have studied regional ground motion scaling in Southern Italy, calibrating also an attenuation relationship for Peak Ground acceleration (PGA) for rock sites. The data set for the area consisted of 3-component stations and the results are valid for the frequency range of 0.25-20 Hz and distances ranged from 20 to about 300 km. For the time domain the data are bandpass filtered within narrow frequency bands to obtain the peak motions. We found

$$Q(f) = 190(f)^{0.65}$$

for the interested area and the geometrical spreading consists of the 2 following segments function:

$$g(r) = \begin{cases} r^{-1.0} & 1 < r < 100km \\ r^{-0.5} & r > 100km \end{cases}$$

I have modelled the excitation terms using the previously determined path term. I have used a Brune point source model with RVT to obtain the stress drop parameter and k. I modelled the excitation terms in two ways: using a few events with a constant stress drop and using all events with known moment magnitudes while each event has a different stress drop parameter. For this reason it was necessary to recompute the moment magnitude for some events as explained in chapter II. In particular I obtained the following values for stress drop and k:

$$\Delta\sigma = 250 \text{ bar} \quad K_0 = 0.040s$$



Using the source and attenuation parameters computed in this study and a set of programs (SMSIM; Boore, 1996) we predicted the expected Peak Ground Acceleration (PGA). The figure 3.8 shows the comparison for magnitude 4.0, 5.0 and 6.0 among the attenuation relations evaluated in this study and the relationships developed by Ambraeseys et al. (1996) for Mediterranean region and Sabetta & Pugliese (1996) for Italy. For our data set it is also evident that the Sabetta and Pugliese (1997) and the Abraseys et al. (1996) attenuation relationships are not useful. In fact they are calibrated on large events and do not consider the ground shaking due to the intermediate magnitudes. The results show the good agreements between the simulation, using the parameter obtained within this study, and the observed PGA values.

Applying the methodology described in fourth chapter we obtained the following functional form and coefficients for predicting PGA values in the study area:

$$\log y = \sum_{i=1}^n a_i E_i + br + c \log r + dS + \varepsilon$$

$$S = \begin{cases} = 1 & \text{for soft soil sites} \\ = 0 & \text{for stiff soil sites} \end{cases}$$

$$\alpha = -3.87$$

$$\beta = 1.22$$

$$b = 0.0024$$

$$c = -1.727$$

$$d = 0.024$$

where  $y$  is peak horizontal acceleration,  $N$  is the number of earthquakes in the data sample, and  $d$  is the closest horizontal distance site to the vertical projection of the



fault rupture [ $r = (d^2+h^2)^{1/2}$ ;  $h$  is obtained from the regression]. Figure 4.9 reports results for  $M=4$ .

Figures 3.8 and 4.9 show some scatter in comparing observed data with the predicted curves. It is due to the fact that our analysis are based on hard rock model. In here we did not taking into account that there are possible effects due to the different path into the crust (Rapolla et al., 2008). In the present work we treated the site as rock sites or at least stiff soils. As a future work it will be interested investigate the behavior of each site by using the technique described in Malagnini et al. 2007 and Mercuri et al. 2007. We those techniques we will able to derive an absolute site term for each station tacking into account the behavior of each component as a function of frequency. In southern Italy, since the crust is very complex both in term of geometry and physical properties, it is clear how the site effects are consequently very important and relevant in order to describe the ground-motion in a particular location The results are relevant for real-time application such us “ShakeMap”.



## REFERENCES

- Akinci, A., L. Malagnini, N. A. Pino, L. Scognamiglio, R. B. Hermann, and H. Eyidogan 2001. High-frequency ground motion in the Erzincan region. Turkey: inferences from small earthquakes, *Bull. Seism. Soc. Am.* **91**, 1446–1455.
- Akinci A., Akyol N., D’Amico S., Malagnini L., Mercuri A. 2006. Ground-Motion scaling in Western Anatolia (Turkey). *Seismological Research Letters*, **77**, 264-265
- Akinci A., D’Amico S., Malagnini L., Mercuri A., Scognamiglio L., 2007. Ground motion scaling in southern Italy: preliminary results. *Seismological Research Letters*, **78**, 279
- Amato, A., Alessandrini, B., Cimini, G., Frepoli, A. and Selvaggi, G.. 1993. Active and remnant subducted slabs beneath Italy: evidence from seismic tomography and seismicity. *Ann. Geot.*.XXXVI(2): 201-214.
- Amato A., P. Montone, 1997. Present day stress-field and active tectonics in Southern Peninsular Italy, *Geophys. J. Int.*, **130**, 519-534.
- Ambraseys, N. N., and K. A. Simpson 1996. Prediction of vertical response spectra in Europe, *Earthquake Eng. Struct. Dyn.* **25**, 401–412.
- Ambraseys, N. N., K. A. Simpson, and J. J. Bommer 1996. Prediction of horizontal response spectra in Europe, *Earthquake Eng. Struct. Dyn.* **25**, 371–400.
- Abrahamson, N. A., & Silva, W. J., 1997. Empirical Response Spectral Attenuation Relations for Shallow Crustal Earthquakes, *Seism. Res. Lett.*, **68** (1), 94-127.
- Anderson, H. and Jackson, J., 1987. The deep seismicity of the Tyrrhenian Sea. *Geophys. J. R. Astron. Soc.*, **91**: 613-637,
- Anderson, J. G., and Y. Lei 1994. Non-parametric description of peak acceleration as a function of magnitude, distance, and site in Guerrero, Mexico, *Bull. Seism. Soc. Am.* **84**, 1003–1017.
- Atkinson, G. M. (1993). Earthquake source spectra and attenuation in southeastern Canada, *Ph.D. Thesis*, University of Western Ontario, London, Ontario.
- Atkinson, G. M. & Boore, D. M., 1995. Ground-Motion Relations for Eastern North America, *Bull. Seism. Soc. Am.*, **85**, 17-30.

- 
- Baisa G., Bruno P.P., Di Fiore V., Rapolla A., 2003. Characterization of shallow volcanoclastic deposits by turning ray seismic tomography: an application to the Naples urban area, *Journal of Applied Geophysics*, **52**, 11-21
- Boccaletti. M., Nicolich, R. and Tortorici, L., 1990. New data and hypothesis on the development of the Tyrrhenian basin. *Palaeogeogr., Palaeoclimatol., Palaeoecol.*, **77**: 15-40.
- Bay, F., D. Fäh, L. Malagnini, and D. Giardini 2003. Spectral shear-wave ground motion scaling for Switzerland, *Bull. Seism. Soc. Am.* **93**, 414–429.
- Barberi, F., Gasparini. P., Innocenti. F. and Vflari, L., 1973. Volcanism of the southern Tyrrhenian Sea and its geodynamic implications. *J. Geophys. Res.*, **78**(23): 5221-5232.
- Bodin, P., L. Malagnini, and A. Akinci 2004. Ground motion scaling in the Kachchh basin, India, deduced from aftershocks of the 2001 *Mw*7.6 Bhuj earthquake, *Bull. Seism. Soc. Am.* **94**, 1658–1669.
- Boore, D. M. & Joyner, W. B., 1991. Estimation of Ground Motion at Deep-Soil Sites in Eastern North America, *Bull. Seism. Soc. Am.*, **81**, 2167-2185
- Boore, D. M., W. B. Joyner, and T. E. Fumal, 1993. Estimation of response spectra and peak acceleration from western North America earthquakes: an interim report, *U.S. Geol. Surv. Open-File Rept. 93-509*, 72 pp.
- Boore, D.M., 1996. SMSIM: Fortran programs for simulating ground motion from earthquakes, version 1.0, *Geol Surv. Open\_file Reprt 96-80A*, 73 pp.
- Boore, D. M., Joyner, W. B., & Fumal T. E., 1997. Equations for Estimating Horizontal Response Spectra and Peak Acceleration from Western North American Earthquakes: A Summary of Recent Work, *Seism. Res. Lett.*, **68** (1), 128-153.
- Boschi E., G. Ferrari, P. Gasparini, E. Guidoboni, G. Smiriglio, G. Valensise, 1995. *Catalogo dei forti terremoti in Italia dal 461 a.C. al 1980*, INGV, roma-SGA Bologna, 973 pp.
- Bottari. A., Broccio, F., Federico, B. and Lo Giudice, E.. 1979. Preliminary crustal model from seismological observations at the Messina Strait network. *Ann. Geofis.* **XXXII**: 91-111.
- Burton. A.N., 1964. Marine levels in South Italy. *Nature*. 203:**1060**.
- Calcagnile. G., Panza. G.F. and Knopoff. L.. 1979. Upper-mantle structure of north-central Italy from the dispersion of Rayleigh v, avcs. *Feclonophysic.*, **56**: 51-63.
- Campell, W. K., 1997. Empirical Near-Source Attenuation Relationships for Horizontal and Vertical Components of Peak Ground Acceleration, Peak Ground



Velocity and Pseudo-Absolute Acceleration Response Spectra, *Seism. Res. Lett.*, **68** (1), 154-179.

Culcagnile. G. and Panza. G.F., 1981. The main characteristics of the lithosphere asthenosphere system in Italy surrounding regions *PAGEOPH*, **119**: 865-879.

Calcagnile, G., D'Ingeo. F., Farrugia, P. and Panza G.F., 1982. The lithosphere in the Central-eastern Mediterranean area. *PAGEOPH*, **120**:389-406.

Campbell, K. W., and Y. Bozorgnia (1994). Near-source attenuation of peak horizontal acceleration from worldwide accelerograms recorded from 1957 to 1993, in *Proc. Fifth U.S. National Conference on Earthquake Engineering*, EERI, Berkeley, California, Vol. 1, 283–292.

Caputo, M., Panza, G.F. and Postpischl, D.. 1970. Deep structure of the Mediterranean Basin. *J. Geophys. Res.* **75**(26): 4919- 4923.

Carrara E., Rapolla A. 1987 . Problematiche geofisiche nella zonazione del territorio in prospettiva sismica e nella caratterizzazione sismica dei siti. *Mem. Soc. Geol. It.* **37**, 533-542.

Cartwright D.E., M.S. Longuet-Higgins, 1956. The statistical distribution of the maxima of a random function, *Proc. R. Soc. London*, **237**, 212-232.

Chouet, B., K. Aki, and M. Tsujiura 1978. Regional variation of the scaling law of earthquake source spectra, *Bull. Seism. Soc. Am.* **68**, 49–79.

Cimini G.B., P. De Gori, A. Frepoli, 2006. Passive seismology in Southern Italy: The SAPTEX array. *Ann. Geophys.*, **49**, 2, 825-840.

Colombi. B., Giese. P., Luongo. G., Morelli, C., Riuscietti. M., Scalascia. S., Schutte. K.G., Stowald. J. and De Visinini. G., 1973. Preliminary report on the seismic refraction profile Gargano-Salerno-Palermo-Pantelleria (1971). *Boll. Geol. Teor. Appl.* **XV**(59): 225-254.

Cristofolini. R., Ghisetti, F., Scarpa. R. and Vezzani, k. 1985. Character of the stress field in the Calabrian Arc and Southern Apennine (Italy) as deduced by geological, seismological and volcanological and volcanological information. *Tectonophysics*. **117**:39-58.

Draper, N. R. & Smith, H., 1966. *Applied Regression Analysis*, Wiley, New York, 407 pp.

Dogliani C., P. Harabaglia, G. Martinelli, F. Mongelli, G. Zito, 1996. A geodynamic model of the Southern Apennines, *Terra Nova*, **8**, 540-547.

- 
- Douglas J., 2003. Earthquake ground motion estimation using strong-motion records: a review of equations for the estimation of peak ground acceleration and response spectral ordinates, *Earth-Science Reviews*, **61**, 43–104
- El All, H. and Giesc. P.. 1978. A geothermal profile between the Adriatic and Tyrrhenian seas: from the Alps, Apennines, Hellenides. In: H. (Gloss, D. Roeder and R. Schimdt (Editors). Geodynamic Investigation along Geotraverses. Schweizerbart. Stuttgart.
- Faccenna, C., T. W. Becker, F.P. Lucente, L. Jolivet, F. Rossetti, 2001. History of subduction and back-arc extension in the central Mediterranean, *Geophys. J. Int.*, **145**, 809– 820.
- Field E.H., McGarr A., Bicknell J., Mori J., Seeber L., Cranswick E., 1990. Attenuation of high frequency shear waves in the crust: measurements from New York state, south Africa and southern California., *J. Geophys.Res.*, **95**, 17441-17454
- Finetti. L. and Del Ben. A.. 1986. Geophysical study, of the Tyrrheuan opening. *Boll. Geofis. Teor. Appl.*, XXVIII(110): 75-155.
- Frazzetta, G., Lanzafame. G. and Villari. L., 1982. Deformazioni e tettonica attiva a Lipari e Vulcano (Eolie). *Mere. Soc. Geol. Ital.*. 24: 293-297.
- Gasparini, C., Iannaccone. G.. Scandone, P. and Scarpa. R.. 1982. Seismotectonics of the Calabrian Arc. *Tectonophysics* 84: 267-286.
- Ghisetti. F. and Vezzani, L., 1982. Different styles of deformation in the Calabrian Arc (Southern Italy): Implications for a seismotectonic zoning. *Tectonophysics*. 55:149-165.
- Ghisetti, F., 1980. Caratterizzazione dei blocchi della Calabria meridionale in base alle velocità di sollevamento nel Plio-Pleistocene: una proposta di zonazione neotettonica. *P.F. Geodinamica. Cons. Naz. Ric.*. Rome, no. 356.
- Ghisetti. F., 1984. Recent deformations and the seismogenic source in the Messina Strait (Southern Italy). *Tectonophysics*, 109: 191-208.
- Ghisetti. F., 1992. Fault parameters in the Messina Strait (Southern Italy) and relations with the seismogenic source. *Tectonophysics*. 210: 117-133.
- Gueguen, E., C. Doglioni, M. Fernandez, 1998. On the post-25 Ma geodynamic evolution of the western Mediterranean, *Tectonophysics*, **298**, 259–269.
- Harmsen, S. 1997. Estimating the diminution of shear-wave amplitude with distance: application to the Los Angeles, California, urban area, *Bull. Seism. Soc. Am.* **87**, 888–903.

- 
- Herrmann, R. B., and L. Malagnini 1996. Absolute ground motion scaling in the New Madrid Seismic Zone, *Seism. Res. Lett.* **67**, 40.
- Herrmann, R. B., and J. Dutt, 1999. High frequency vertical ground motion in the Pacific Northwest using PNSN data, *Seism. Res. Lett.* **70**, 216.
- Herrmann, R. B., and Ammon C. J., 2002. Source Inversion, *Computer Programs in Seismology*, Version 3.30 (<http://www.eas.slu.edu>), pp. 98
- Jeon Y.S., R.B Herrmann, 2004. High-frequency ground-motion scaling in Utah and Yellowstone. *Bull. Seism. Soc. Am.* **94**, 1644-1657.
- Joyner, W. B. & Boore, D. M., 1981. Peak Horizontal Acceleration and Velocity from Strong-Motion Records Including Records from the 1979 Imperial Valley, California, Earthquake, *Bull. Seism. Soc. Am.*, **71** (6), 2011-2038.
- Joyner, W. B. & Boore, D. M., 1993. Methods for the Regression Analysis of Strong-Motion Data, *Bull. Seism. Soc. Am.*, **83** (2), 469-487.
- Kramer S.L. (1996). *Geotechnical Earthquake Engineering*. Prentice Hall, Upper Saddle River, NJ.
- King J.L., Tucker B.E., 1984. Observed variations of earthquake motion across a sediment filled valley, *Bull. Seism. Soc. Am.*, **74**, 137-151
- Lavecchia. G., 1988. The Tyrrhenian Apennines system structural setting and seismotectogenesis. *Tectonophysics*, **147**: 263-296.
- Locardi, E., 1988. The origin of the Apenninic arcs. *Tectonophysics*, **146**: 105-123.
- Loddo, M. and Mongelli, F., 1979. Heat flow in Italy. *PAGEOPH*, **117**: 135-149.
- Malagnini, L., R. B. Herrmann, and M. Di Bona 2000a. Ground-motion scaling in the Apennines (Italy), *Bull. Seism. Soc. Am.* **90**, 1062–1081.
- Malagnini, L., R. B. Herrmann, and K. Koch 2000b. Regional ground motion in scaling in Central Europe, *Bull. Seism. Soc. Am.* **90**, 1052– 1061.
- Malagnini, L., and R. B. Herrmann 2000c. Ground motion scaling in the region of the 1997 Umbria-Marche earthquake (Italy), *Bull. Seism. Soc. Am.* **90**, 1041–1051.
- Malagnini, L., A. Akinci, R. B. Herrmann, N. A. Pino, and L. Scognamiglio 2002. Characteristics of the ground motion in northeastern Italy, *Bull. Seism. Soc. Am.* **92**, 2186–2204.



Malagnini L., K. Mayeda, Uhrhammer R., A. Akinci, R.B Herrmann, 2007. A regional Ground-motion excitation/attenuation model for the San Francisco Region. *Bull. Seism. Soc. Am.* **97**, 843-862.

Malagnini, L., K. Mayeda, R. Uhrhammer, A. Akinci, and R.B. Herrmann, 2007. A regional ground motion excitation/attenuation model for the San Francisco region, *Bull. Seism. Soc. Am.*, 97; 3; p. 843-862; DOI: 10.1785/0120060101.

Malagnini, L., K. Mayeda, A. Akinci, and P.L. Bragato, 2004. Estimating absolute site effects, *Bull. Seism. Soc. Am.*, 94, 1343-1352

Malinverno A., W.B.F. Ryan, 1986. extension in the Tyrrhenian Sea and shortening in the Apennines as a result of arc migration driven by sinking of the lithosphere, *Tectonics*, **5**, 227-245.

Mantovani, E., Babbucci, D., Albarello, D. and Mucciarelli, M., 1990. Deformation pattern in the Central Mediterranean and behavior of the African/Adriatic promontory. *Tectonophysics*, **179**: 63-79.

Marone C. and Scholts C. H., 1998. The depth of seismic faulting and the upper transition from stable to unstable slip regimes, *Geophys. Res. Lett.*, **15**, 621-624.

Martini, M. and Scarpa, R., 1982. Italian earthquakes since 1900. In: Proc. E. Fermi Summer School in Geophysics, Varenna. Springer, Berlin, pp. 479-492.

Masclé, J., Kastens, K., Auroux C. and Leg 107 Scientific Party. 1988. A land-locked back-arc basin: preliminary results from ODP Leg 107 in the Tyrrhenian Sea. *Tectonophysics*, 146: 149-162.

Mercuri A., Malagnini L., Scognamiglio L., Milana G., Akinci A., 2007. Absolute site effects in the Abruzzo region – Italy, *Seismological Research Letters*, **78**, 2, 278-279.

Moya A., Aguirre J., Irikura K., 2000. Inversion of source parameters and site effects from strong motion records using genetic algorithms, *Bull. Seism. Soc. Am.* **90**, 977-992

Mongelli, F., Loddo, M. and Calcagnile, G., 1975. Some observations on the Apennines gravity field. *Earth Planet. Sci. Lett.*, 24: 385-393.

Mongelli F., Zito, G., Ciaranfi. N. and Pieri, P., 1989. Interpretation of heat flow density of the Apennine chain, Italy. *Tectonophysics*, 164: 267-280.

Morelli, C., Giese, P., Cassinis, R., Colombi. B., Guerra, I., Luongo, G., Scarscia, S. and Schutte, K.G., 1975. Crustal structure of Southern Italy. A seismic refraction profile between Puglia-Calabria-Sicily. *Boll. Geofis. Teor. Appl.*, **17**: 182-210.



- Morasca P., L. Malagnini, Akinci A., Spallarossa D., Herrmann R.B., 2006. Ground motion scaling in the western Alps. *J. Seismol.*, **10**, 315-333.
- Mulargia, F. and Boschi, E., 1982. The 1908 Messina earthquake and related seismicity. In: Proc. E. Fermi Summer School in Geophysics. Varenna. Springer, Berlin, pp. 493-518.
- Mulargia, F., Baldi, P., Achilli, V. and Broccio. F., 1984. Recent crustal deformation and tectonics of the Messina Strait area. *Geophys. J. R. Astron. Soc.*, **76**: 369-381.
- Neri G., Caccamo D., Cocina C., Montalto A., 1996. Geodynamic implications of earthquake data in the southern Tyrrhenian sea. *Tectonophysics*, **258**, 233-249
- Nur, A., Dvorkin, J., Mavko, G. and Ben-Avraham. Z., 1993. Speculations on the origin and fate of backarc basins. *Ann. Geofis.*, **XXXVI**(2): 155-163.
- Ortega, R., R. B. Herrmann, and L. Quintanar 2003. Earthquake ground-motion scaling in Central Mexico between 0.7 and 7 Hz, *Bull. Seism. Soc. Am.* **93**, 397–413.
- Panza, G.F., Prozorov. A.G. and Suhadolc, P., 1990. Lithosphere structure and statistical properties of seismicity in Italy and surroundings regions. *J. Geodyn.*, **12**: 189-215.
- Patacca. E. and Scandone, P., 1989. Post-Tortonian mountain building in the Apennines. The role of the passive sinking of a relic lithospheric slab. In: Proc. Accad. Lincei Congr., **80**: 157-176.
- Patacca, E., Sartori, R. and Scandone, P., 1990. Tyrrhenian basin and Apenninic arcs: kinematic relations since late tortonian times. In: 75th Congr. Soc. Geol. Ital., Milano, September 1990. *Mere. Soc. Geol. Ital.*, **45**:425-451.
- Peterschmitt, E., 1956. Quelques Donnes Nouvelles sur les Seismes Profonds de la Mer Tyrrhenienne. *Ann. Geofis.* **9**:305 334.
- Pino, N. A., L. Malagnini, A. Akinci, L. Scognamiglio, R. B. Herrmann, G. Stavrakakis, and G. Chouliaras 2001. Ground motion scaling relationships for mainland Greece and Crete, *Seism. Res. Lett.* **72**, 258.
- Rapolla, A.; Bais, G.; Bruno, P. P. et al., 2002. Earth modeling and estimation of the local seismic ground motion due to site geology in complex volcanoclastic areas. *Annales of Geophysics*.
- Rapolla A. 2004 . Procedure per la valutazione della pericolosità sismica (microzonazione e risposta sismica locale) in Campania alla luce delle nuove normative. *Boll. Ord. Reg. Geologi della Campania* **4**, Napoli.



Rapolla A., Bais G., Bruno P.P. & Di Fiore V. 2002 . Earth modelling and estimation of the local seismic ground motion due to site geology in complex volcanoclastic areas. *Annals of Geophysics* 45(6), 779-790.

Rapolla A., Akinci A., Bruno P. P., D'Amico S., Di Fiore V., Malagnini L., Maschio L., Paoletti V., Secomandi M., Vietri A., 2008. La pericolosità sismica: dalla classificazione sismica alla microzonazione dei territori comunali, alla risposta sismica del sito. Liguori Editore, in press

Raoof, M., R. B. Hermann, L. Malagnini, 1999. Attenuation and excitation of three-component ground motion in southern California, *Bull. Seism. Soc. Am.* **89**, 888–902.

Rehault, J.P., Moussat. E. and Fabbri, A., 1987. Structural evolution of the Tyrrhenian back-arc basin. *Mar. Geol.*, 74:123-150.

Sabetta, F., and A. Pugliese (1987). Attenuation of peak horizontal acceleration and velocity from Italian strong-motion records, *Bull. Seism. Soc. Am.* **77**, 1491–1511.

Sabetta, F., and A. Pugliese (1996). Estimation of response spectra and simulation of nonstationary earthquake ground motion, *Bull. Seism. Soc. Am.* **86**, 337–352.

Sadigh, K., 1997. Attenuation Relations for Shallow Crustal Earthquakes Based on California Strong Motion Data, *Seism., Res. Lett.*, **68** (1), 180-189.

Savelli, C., 1988. Late Oligocene to Recent episodes of magmatism in and around the Tyrrhenian Sea: implications for the processes of opening in a young inter-arc basin of intra-orogenic (Mediterranean) type. *Tectonophysics*. **146**, 163-181.

Scandone, P, and Patacca, E., 1984. Tectonic evolution of the Central Mediterranean area. *Ann. Geophys.*, **2**, (2): 139-142.

Scarpa, R., 1982. Travel-time residuals and three-dimensional velocity structure of Italy. *PAGEOPH*, 120: 583-606.

Scherbaum F., Schmedes J., Cotton F., 2004. On the Conversion of Source-to-Site Distance Measures for Extended Earthquake Source Models, *Bulletin of the Seismological Society of America*, **94**, 3, 1053-1069

Scognamiglio L., Malagnini L., Akinci A., 2005. Ground motion scaling in eastern sicily, Italy. *Bull. Seism. Soc. Am.* **95**, 568-578.

Sormeville P. G., Smith N. F., Graves R. W., Abrahamson N. A., 1997. Modification of empirical strong ground motion attenuation relations to include the amplitude and the duration effects of the rupture directivity., *Seismological Research Letters*, **68**, 199-222



Stield J.H., Tumarkin A. G., Archuleta R. L., 1996. What is a reference site, *Bull. Seism. Soc. Am.* **86**, 1733-1748

Steinmetz, L., Ferrucci, F., Him, A., Morelli, C. and Nicolich, R., 1983. A 550km long Moho traverse in the Tyrrhenian Sea by OBS recorded Pn waves. *Geophys. Res. Lett.*, 10:428-431.

Toro, G. R. & McGuire, R. K., 1987. An Investigation into Earthquake Ground Motion Characteristics in Eastern North America, *Bull. Seism. Soc. Am.*, 77, 468-489.

Yazd, M. R. S. 1993. Ground motion studies in the Southern Great Basin of Nevada and California, *Ph.D. Thesis*, Saint Louis University.

Wald D., Worden B., Quitoriano V., Pankow K.L., 2005. Shake Map manual: technical manual, user's guide, and software guide. U.S. Geological Survey Techniques and Methods, book 12, section A, 132 pp.

Weisberg, S., 1980. *Applied Linear Regression*, Wiley, New York, 282 pp.

Van Dijk, J. and Okkes. M., 1991. Neogene tectonostratigraphy and kinematics of Calabrian basins; implications for the geodynamics of the Central Mediterranean. *Tectonophysics*, 196: 23-60.